FOURIER SERIES BASED MODEL REFERENCE ADAPTIVE CONTROL

A THESIS SUBMITTED TO
THE GRADUATE SCHOOL OF NATURAL AND APPLIED SCIENCES
OF
MIDDLE EAST TECHNICAL UNIVERSITY

BY

RÜŞTÜ BERK GEZER

IN PARTIAL FULFILLMENT OF THE REQUIREMENTS
FOR
THE DEGREE OF MASTER OF SCIENCE
IN
AEROSPACE ENGINEERING

AUGUST 2014

Approval of the thesis:

FOURIER SERIES BASED MODEL REFERENCE ADAPTIVE CONTROL

submitted by **RÜŞTÜ BERK GEZER** in partial fulfillment of the requirements for the degree of **Master of Science in Aerospace Engineering Department, Middle East Technical University** by,

Prof. Dr. Canan Özgen _____
Dean, Graduate School of **Natural and Applied Sciences**

Prof. Dr. Ozan Tekinalp _____
Head of Department, **Aerospace Engineering**

Assist. Prof. Dr. Ali Türker Kutay _____
Supervisor, **Aerospace Engineering Department, METU**

Examining Committee Members:

Prof. Dr. Ozan Tekinalp
Aerospace Engineering Department, METU _____

Assist. Prof. Dr. Ali Türker Kutay
Aerospace Engineering Department, METU _____

Prof. Dr. M. Kemal Leblebicioğlu
Electrical and Electronics Engineering Department, METU _____

Assoc. Prof. Dr. İlkay Yavrucuk
Aerospace Engineering Department, METU _____

Dr. Osman Merttopçuoğlu
Roketsan Missiles Inc. _____

Date: _____

I hereby declare that all information in this document has been obtained and presented in accordance with academic rules and ethical conduct. I also declare that, as required by these rules and conduct, I have fully cited and referenced all material and results that are not original to this work.

Name, Last Name: RÜŞTÜ BERK GEZER

Signature :

ABSTRACT

FOURIER SERIES BASED MODEL REFERENCE ADAPTIVE CONTROL

GEZER, RÜŞTÜ BERK
M.S., Department of Aerospace Engineering
Supervisor : Assist. Prof. Dr. Ali Türker Kutay

August 2014, 91 pages

Any signal in nature includes periodic signals with different frequencies and weightings. Therefore, any signal can be represented using summation of simple periodic functions. Representation of signals with periodic functions is called Fourier series representation. This powerful utility of the Fourier series is aimed to be used for adaptive control. In the direction of this aim, a novel approach for model reference adaptive control is proposed in this thesis.

The Fourier series based model reference adaptive control represents an alternative for uncertainty parametrizations used in model reference adaptive control. Commonly designed MRAC schemes use known functions of system variables or in some cases neural networks for uncertainty parametrization. In this study, these parametrization methods are replaced with Fourier series.

The sine and cosine elements; which are functions of time with periods that are multipliers of precessors, are used as basis functions. An adaptation law for estimating the weightings of the periodic functions is derived using Lyapunov stability principle. The adaptive input is calculated by multiplying the periodic basis functions and the estimated weights.

In this thesis, two other alternative for the proposed method are examined. These alternatives are model following control and basic model reference adaptive control

that uses known functions of system variables. These controllers are designed for a sample problem. Robustness properties of the model following controller is analyzed. Performances of these controllers are inspected under defined and random disturbances, and the results are compared with the proposed controller.

The performance of the Fourier series based MRAC scheme is shown to be satisfactory. The comparison of the results indicates that the proposed controller gives better disturbance rejection for the same performance level.

Keywords: Adaptive Control, Fourier Series, Unknown Uncertainty, Disturbance Rejection

ÖZ

FOURİER SERİSİ TABANLI MODEL REFERANS ADAPTİF KONTROL

GEZER, RÜŞTÜ BERK
Yüksek Lisans, Havacılık ve Uzay Mühendisliği Bölümü
Tez Yöneticisi : Yrd. Doç. Dr. Ali Türker Kutay

Ağustos 2014 , 91 sayfa

Doğada herhangi bir sinyal, farklı frekanslara ve ağırlıklara sahip periyodik sinyaller içerir. Bu nedenle, herhangi bir sinyal basit periyodik fonksiyonların toplamı ile temsil edilebilir. Sinyallerin periyodik fonksiyonlar ile gösterimine Forier serisi gösterimi denir. Fourier serilerinin bu güçlü özelliğinin adaptif kontrolcü yapıları için kullanılması hedeflenmektedir. Bu hedefin doğrultusunda, bu tez çalışmasında Fourier serisi tabanlı model referans adaptif kontrol yöntemi sunulmaktadır.

Fourier serisi tabanlı model referans adaptif kontrol yöntemi, model referans adaptif kontrolde kullanılan belirsizlik parametrizasyonuna bir alternatif sunmaktadır. Genelde tasarlanan MRAC yapıları belirsizlik parametrizasyonu için sistem değişkenlerinin bilinen foksiyonlarını ya da bazı durumlarda yapay sinir ağlarını kullanmaktadırlar. Bu çalışmada, bahsi geçen belirsizlik parametrizasyonları Fourier serisi ile değiştirilmektedir.

Taban fonksiyonu olarak, periyodları birbirinin çarpanı olan zaman fonksiyonu sinüs ve cosinüs elemanları kullanılmaktadır. Lyapunov kararlılık presibi kullanılarak, bir tahmini ağırlık güncelleme kanunu türetilmektedir. Adaptif kontrolcü girdisi bu periyodik taban fonksiyonları ile tahmini ağırlıkların çarpılması ile hesaplanmaktadır.

Bu tez çalışmasında önerilen methodun yanında iki farklı alternatif de incelenmektedir. Bu alternatifler; model takibi ile kontrol ve sistem değişkenlerinin bilinen fonksi-

yonlarını kullanan temel model referans adaptif kontroldur. Bu kontrolcüler örnek bir sistem için tasarlanmaktadır. Model takip eden kontrolcünün gürbüzlük özellikleri analiz edilmektedir. Bu kontrolcülerin performansları tanımlı ve rastgele bozucular altında incelenmekte ve önerilen kontrolcü ile karşılaştırılmaktadır.

Fourier series tabanlı MRAC yönteminin performansının tatmin edici olduğu gösterilmektedir. Karşılaştırma sonuçları, önerilen kontrolcünün daha iyi bir belirsizlik giderme karakteri olduğunu ortaya koymaktadır.

Anahtar Kelimeler: Adaptif Kontrol, Fourier Serisi, Bilinmeyen Belirsizlik, Bozucu Etki Giderme

To my family and my lovely wife

ACKNOWLEDGMENTS

I would like to express the deepest appreciation to my supervisor Asst. Prof. Dr. Ali Türker Kutay for his guidance and interest throughout this study. His enthusiasm, encouragement and faith in me throughout have been extremely helpful. I wish to express my sincere thanks to my committee members Prof. Dr. Ozan Tekinalp, Prof. Dr. Kemal Leblebicioğlu, Assoc. Prof. Dr. İlkay Yavrucuk, Dr. Osman Merttopçuoğlu for their contribution and comments on this study.

I would like to thank Alper Kahvecioğlu for his helps and support; my colleagues Gökcan Akalın and Suzan Kale for their encouragement and all the discussions we have made.

I am also grateful to Müge Gülbiter and Ahmet Gülbiter for their psychological support.

Above all, I would like to thank my parents Öznur Gezer and Turgay Gezer for their endless love, encouragement and support in all aspects all through my life. I am also thankful to my sister Pervin Gizem Gezer for her invaluable friendship.

Last but not the least important, I owe more than thanks to my dear wife Miray Gezer.

This work is also supported by TÜBITAK-BIDEB National Graduate Scholarship Programme for Ms (2210).

TABLE OF CONTENTS

LIST OF FIGURES

FIGURES

LIST OF ABBREVIATIONS

CAS	Control Actuator System
FSE	Fourier Series Expansion
MFC	Model Following Control
MRAC	Model Reference Adaptive Control

CHAPTER 1

INTRODUCTION

Automatic control of a dynamic system is a topic that has been studied for more than a century. The centrifugal governor for steam engine speed control which was conducted by James Clerk Maxwell in 1868 [34] can be taken as the beginning of automatic control. One of the most famous applications of the automatic control is the flight control system of the Wright Brothers' first flight in 1903. In 1922, Minorsky showed that differential equations describing the steering ships dynamics can be used for stabilization [35, 17]. In 1932, a plain method for determining the stability of closed-loop systems was found by Nyquist [41]. In the 1940s, the frequency response approach to design close-loop control systems was developed by Bode [58]. The root-locus method was introduced in 1954 by Walter R. Evans, which forms the core of the classical control theory together with the Bode diagram. These tools are used for the design of the closed-loop control systems. The plants worked on with classical control theory are single-input-single-output plants.

The designed controllers using the classical control techniques were able to satisfy the given requirements, but they were not shown to be optimal in any perspective. But, controllers that use control resources optimally is a logical interest for controller design; so, some sort of optimality was needed for controllers. Also, while the frequency response analysis methods are strong tools for designs of single-input-single-output systems, as plants started to have more inputs and outputs, the need for the control of multiple-input-multiple-output systems has arisen. In order to meet these interests, modern control methods have been developed. The full state feedback method which uses the state-space form of the linear dynamical systems make controller de-

sign for multiple-input-multiple-output systems possible. Moreover, this method has carried the design procedure from the frequency domain to the time domain. This gave insight to the designer about time response of the controller but needed a lot of computation. This improvement brought by the modern control theory is applicable with the availability of the digital computers. The optimal control theory for calculating optimal usage of the control resources was developed in order to overcome the optimality problem of the classical control theory [47, 49].The works of Pontryagin and Bellman established the basis of modern control theory [47, 49, 6].

Both classical and modern control theories need a linear model representing the system dynamics. It is hard to linearize dynamical models of highly agile aircraft, missiles and other autonomous air vehicles that operate in a wide range of conditions, since these vehicles have extremely nonlinear dynamics. The interest in designing autopilots for such vehicles motivated the development of adaptive control theory, and first steps were taken to automatically adjusting the controller parameters to changing aircraft dynamics during the flight [20]. Several studies on gain scheduling, model reference adaptive control, and self tuning control were conducted in 1960s [3, 60, 26]. There were some stability problems which arose with the usage of the developed adaptive control theory. Several researchers studied instability of and modifications on the adaptation mechanism of the adaptive control [23, 24, 25, 29, 37, 45]. After these studies, several improvements were added to the theory, and efforts to develop the adaptive control theory have continued to the present day.

1.1 Literature Survey

Adaptive control theory can be organized in three methods. These methods are the gain scheduling, the self tuning control and the model reference adaptive control.

The gain scheduling method comes out of the simple idea of changing the gains of a controller according to variations in the operation regime. Separate fixed gain controllers are designed for various operation points, and the gains of the controllers are changed according to subsidiary measurements. By this method, it has become possible to overcome parameter variations in the system dynamics by scheduling the

controller gains. This method is very strong in the cases where the parameters of the plant changes with respect to a subsidiary variable which is available for measurement. The Mach number or dynamic pressure are such subsidiary variables for forward flight applications like aircraft or missile autopilots. Some examples of the gain scheduling approach used in the practice can be found in literature [36, 54, 1, 48]. An excessive explanation of the method is given in [50]. The block diagram of the gain scheduling approach is shown in the Figure 1.1.

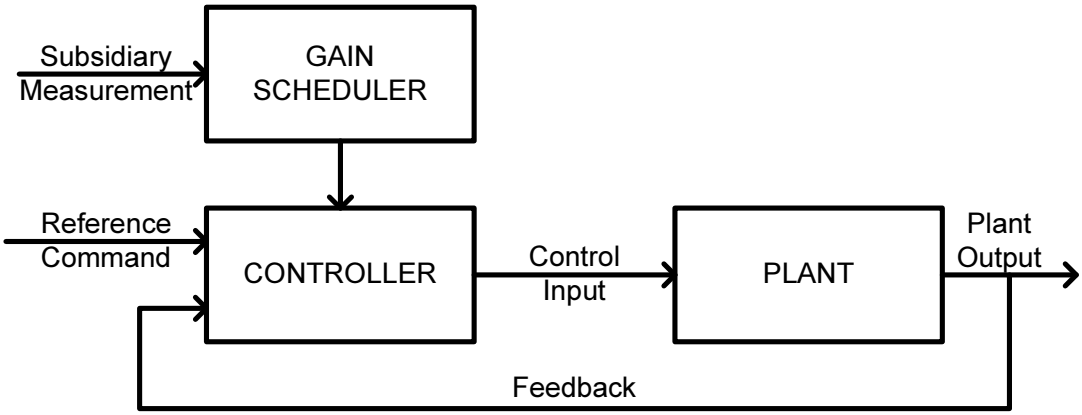

Figure 1.1: Block diagram of Gain Scheduling approach.

The idea of gain scheduling is easy to implement and adaptive to variations in the system parameters that can be modeled prior to the application. However, this approach is an open-loop adaptive design procedure and can not adapt itself to unpredicted variations and out of design conditions. Also, in order to have a controller that is tuned over all the application region, an enormous amount of design points might be needed. For example, anti-air missiles can fly in a wide range of Mach numbers and altitudes. Moreover, the inertia, mass and center of gravity of missiles change dramatically in flight. These variations of the system can be modeled, and for every selected trim point a controller design can be conducted. Finally, the resulting designs can be joint each other by the use of gain scheduling method. The disadvantage of this procedure is that it consumes plenty of engineering man-hours. Even so, the gain scheduling approach is one of the powerful adaptive control approaches that is widely used in practice.

Another main approach of adaptive control is the self tuning control. In self tuning control, an analytical relation between the plant parameters and controller gains is

evaluated. During the application, the varying system parameters are identified by using a parameter identification technique. These identified system parameters are used to calculate adaptive controller gains via the analytical relation evaluated. Several identification methods such as least squares, maximum likelihood and extended Kalman filtering can be used for parameter identification [16, 59]. Furthermore, various analytical procedures which use system parameters for control design can be used for self tuning control, for example, gain-phase margin design, linear quadratic regulator, and so fort [42, 12]. The block diagram of the self tuning control method is shown in the Figure 1.2.

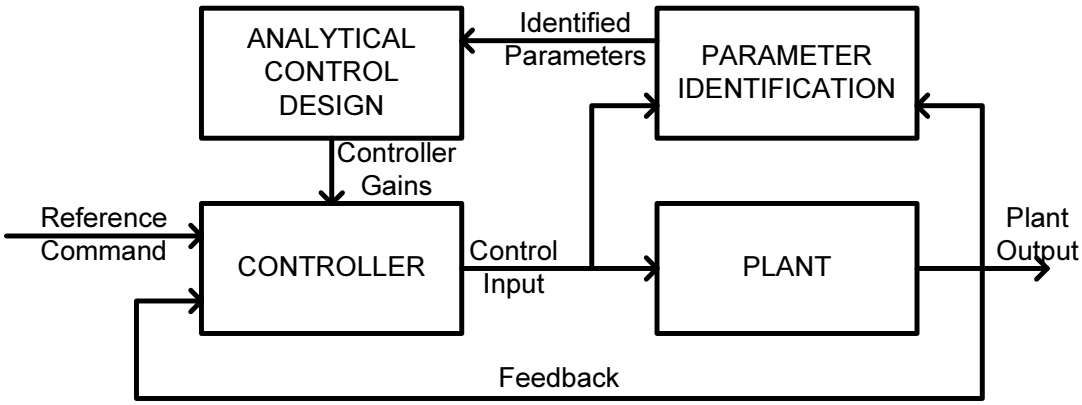

Figure 1.2: Block diagram of Self Tuning Control.

This approach was originally proposed in [26] and explained clearly in [4]. In [21], self tuning control was applied to a rotorcraft for terrain following flight. Various applications of the self tuning control on spacecrafts were demonstrated in [52, 51, 13].

Model reference adaptive control (MRAC) is another method in the adaptive control theory which was developed in 1950s [60, 43, 5]. The main idea of MRAC is to define a desired response by a reference model, and make the plant output to match the reference model output with the use of the adaptive element. In this approach, the error between the reference output and the plant output is used to drive the adaptation law. By the adaptation law, an adaptive control input is calculated, and this input is combined with the nominal controller input. The adaptive part of the MRAC is active if the plant output drifts away from the reference model output and is passive if two outputs are close to each other. In this sense, MRAC is an augmenting controller on

a nominal controller of any kind. The block diagram of the model reference adaptive control is shown in the Figure 1.3.

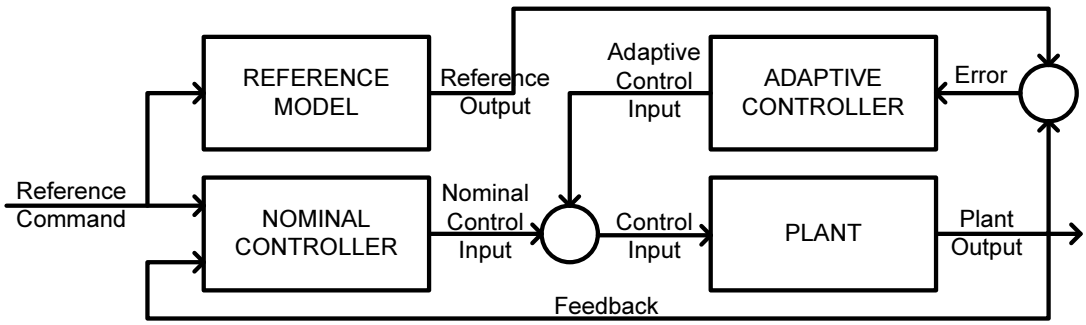

Figure 1.3: Block diagram of Model Reference Adaptive Control.

MRAC can be separated into two parts. One of them is the reference model that is used to define the desired performance of the closed-loop system. The other one is the adaptive part of the MRAC, which can be divided into two main components. These are the uncertainty parametrization and the weight update law. The uncertainty parametrization component parametrizes the uncertainty in a way that, it can be represented by multiplication of some ideal constant weights and variable functions. The weight update law component forms the update equation for the weight estimation of the constant ideal weights of the uncertainty parametrization.

The weight update law depends on the Lyapunov stability property [32, 33]. The first studies on the stability of MRAC weight update law with the use of Lyapunov stability were in [7, 44]. Many modifications to the weight update law can be found in the literature. A damping pole has been added to the weight update law by the σ modification [22]. A variable damping character has been introduced by the e modification [37] where the damping increases as the norm of the error between the reference model and the plant output increases. A projection modification on the weight update law that uses a bound depending on the Lyapunov equation to project the growing weights has been presented in [46]. An optimal control theory based modification on weight update law has been given in [39, 40].

Adaptive loop recovery method protects the frequency domain characteristics of the closed-loop design even when the plant is under disturbance [9, 10]. A stiffness term to the weight update law has been added by the κ modification [27]. A Kalman

filter modification has been developed for weight update law which uses Kalman filter optimization method [63]. Possible effects of the discontinuous disturbances on the plant, such as, drop of a payload, have been smoothed by the derivative free modification on weight update law of MRAC. The derivative free modification has been presented in [62, 64, 65] A modification on weight updated depending on least squares gradient method has been shown in [38]. So, there are plenty of studies on the modifications and improvements of the weight update law.

For MRAC, the uncertainty on the system is needed to be modeled by some functions. The variation of the disturbance acting on the system is modeled using a multiplication of some ideal constant weights and variable functions. This uncertainty modeling is called as uncertainty parametrization. There are several methods used in the literature for uncertainty parametrization. The most general but less realistic method to parametrize the uncertainty is using known functions of system variables. This approach assumes that the unmodeled nonlinear or unknown linear parts of the system dynamics are acting as uncertainties on the plant to be controlled. And also, it assumes that these uncertainties has a known structure formed by the system variables. Therefore, the structure of the uncertainties is known to be as functions of system variables and the unknown ideal weights of these functions. This type of uncertainty parametrization applications has been used in numerously studies, some of which are [46, 9, 10, 31, 39, 40, 64, 61, 65]. Among the example references given for the use of functions of system variables as uncertainty parametrization, two [46, 65] of them use the input variable in these functions. Others form the uncertainty parametrization by functions of states of the system only. This distinction has a role which is explained in the next section 1.2.

For the parametrization of the uncertainty, another frequently used method is modeling the uncertainty by universal function approximators. The universal function approximator used for the uncertainty parametrization is the neural networks. There are two types of neural networks used for uncertainty modeling. One of them is a neural network using radial bases functions in a single layer. Example studies using radial basis functions for uncertainty parametrization can be found in [30, 15]. The other type of neural network used for uncertainty parametrization is sigmoidal activation function based layers. Studies using sigmoidal activation functions for neural

networks are shown in [8, 14, 27, 11, 63, 19]. Both neural network types are driven by the system states. So, the uncertainty parametrization by using neural networks also depends on system states only.

The difference between the parametrization via known functions of system variables and neural networks as universal approximators is, the uncertainty model is restricted to a predefined model in one, but can be in any form of system states in the other. If the uncertainties on the system are guarantied to have a certain model, then using the known functions of system variables is advantageous. If not, then universal approximators work fine.

1.2 Contribution of this Thesis

The study represented in this thesis proposes a novel method for uncertainty parametrization for model reference adaptive control scheme. The proposed method is estimating the disturbance using periodic functions, and it is called Fourier series based model reference adaptive control.

Every periodic event in nature can be decomposed into simple periodic functions. Summation of simple sine and cosine functions with frequencies that are integer divisors of a selected period are used to represent the periodic event. In the summation, every single periodic function has its own weight, so the total sum gives the value corresponding the event itself.

This property of nature is used for adaptive control to parametrize the disturbance and uncertainty on the system. The parametrization method used depends on Fourier series. The periodic functions are functions of time, and the adaptation mechanism tries to find the correct weightings that represent the disturbance on system. So, by using this information obtained by the Fourier series, the control input is updated with an adaptive input.

A question may arise that if the disturbance and uncertainty on the system are not periodic, then how this method is assumed to be working. This question is valid for infinitely operating systems. However, for systems with finite operation time, a proper

period for the Fourier series that is used in the adaptive controller, can be selected. In other words, any signal that is defined in a finite time can be represented using a longer period and assumed to be periodic with the selected period. The corresponding Fourier series expansion represents the signal for its operating time correctly.

It is important to highlight some advantages of the proposed Fourier series based model reference adaptive control method. There are two prominent advantages of the method. Both of the advantages contained in the uncertainty parametrization scheme of the proposed method. These are omitting assumptions for the structure of the uncertainty, and system state independency and only being function of time of the uncertainty parametrization.

In most of the studies a certain model for the structure of the disturbance acting on the system is assumed. This assumption covers all the studies that are using known functions of system variables for the parametrization. By this assumption, the adaptive element is forced to find the disturbance in the set defined for the parametrization. For the case the disturbance does not hold with the pre-assumed structure, the controller has problems to reject all of the disturbance. In order to get rid of this weakness of the adaptive controllers, an uncertainty parametrization by using Fourier series as universal approximator is proposed. This is the first significant advantage of the idea. This advantage is also applies for the neural network based adaptation schemes. However, the next advantage carries the proposed method one step further.

The second advantage of the proposed method is that the uncertainty parametrization is independent from the system states. This situation produce two aspects.

One of them, since the uncertainty parametrization part of the adaptive element is not a function of the system states, the consistent perturbation need of the learning mechanism is eliminated. Since, the periodic elements in the parametrization are functions of time, they are perturbed during the all operation time. Therefore, adaptation of the system to any error on the system does not stop.

The second aspect of being independent from the system states of the proposed uncertainty parametrization is that the algebraic loop problem of the adaptive element is eliminated. For the case, when both the input and the system states excites un-

modeled effects on the system as disturbances, and the adaptive element is formed as function of these system variables, then an algebraic loop occurs. The controller input; which includes the adaptive input correction, effects the disturbance on the system. Then, the adaptive input correction is calculated by using the pre-assumed function of system variables which includes functions of control input. Hence, the adaptive control input becomes dependent to itself which means an algebraic loop occurs. This unwanted phenomena is omitted by using a uncertainty parametrization which is independent of system states and inputs, and capable to reject the disturbance on the system.

To sum up, a novel approach for uncertainty parametrization used in the model reference adaptive control is proposed in this study.

1.3 Thesis Structure

In the first chapter 1, a brief introduction to the history of the automatic control is given. Then, a literature survey including three main sections of the adaptive control methods is presented. Finally, the contribution of this thesis is expressed.

The second chapter 2 is called model following control. In this chapter, the model following control method belongs in the modern controller schemes is discussed. First, a sample system for designing the controller is set. Then, design of the model following controller is conducted. Then, robustness analysis that includes calculating disturbance rejection and noise filtering performances of the model following controller is done. Then, the command following performance of the controller is examined in simulation examples section with step and sine wave commands. Finally, a challenging disturbance case where the disturbance is not only function of the system states is exerted.

In the third chapter 3, the basic model reference adaptive control is examined. The adaptive control used in this chapter uses known functions of the system states as uncertainty parametrization. First, the MRAC method is represented. Then, the command following performance of the designed MRAC is inspected with simulations for challenging disturbance case.

In the fourth chapter 4, the novel method; Fourier series based model reference adaptive control is proposed. First, the stability proof of the proposed method is represented. Then, the command following performance of the Fourier series based MRAC is examined. The performance of the controller is compared with the other two controllers explained in the previous chapters.

In the final chapter 5, the thesis is concluded.

CHAPTER 2

MODEL FOLLOWING CONTROL

Controlling a dynamical system is setting the transient and steady-state responses of that system. The transient response of a system can be set to a desired response if there is a predefined character for the response of that system. For example, the desired transient responses for channels and modes of the airplane control are defined by the handling qualities [55]. Airplane controllers are designed to imply these handling qualities to the airplane response.

There are different classical and modern control approaches for controlling dynamic systems with desired responses. The model following control (MFC) is the most explicit one, when the desired response is taken as primary design objective. In the MFC, the desired response is defined as a reference model in the controller, and the system output is forced to behave like the reference model output. The MFC method has been established with the improvements in the modern control theory and some examples can be found in [55, 57, 2, 28, 56].

In this chapter, first a sample system model is defined in 2.1 for use of the rest of the study. Secondly, the MFC architecture is presented in 2.2 and the design is discussed. Thirdly, the robustness properties of the MFC is examined in 2.3 by frequency domain tools. In 2.4, linear simulation examples are presented, and finally in 2.5 a challenging unknown external disturbance effect on the system is inspected.

2.1 Sample System Model

In order to represent the controller methods discussed in this study, a simple system model is defined. This system model has two states. One of them is directly driven by the input, and the other one is the integral of the first state. The equation regarding the system model is

$$\begin{aligned} \dot{x}_1(t) &= u(t) + \delta(x(t), t), \quad x_1(0) = x_{10}, \quad t \in \mathbb{R}_+ \\ \dot{x}_2(t) &= x_1(t), \qquad\qquad\quad x_2(0) = x_{20}, \quad t \in \mathbb{R}_+. \end{aligned} \tag{2.1}$$

This is the rolling motion model of a slender delta wing with wing rock dynamics defined in [53, 66]. The first state $x_1(t) \in \mathbb{R}$ is the roll rate, and the second state $x_2(t) \in \mathbb{R}$ is the roll angle of the slender delta wing. The control input on the system is shown with $u(t) \in \mathbb{R}$. The equation (2.1) can be rewritten in matrix form as

$$\dot{x}(t) = Ax(t) + B(u(t) + \delta(x(t), t)) \tag{2.2}$$

where $A = \begin{bmatrix} 0 & 0 \\ 1 & 0 \end{bmatrix}$ is the system matrix, and $B = \begin{bmatrix} 1 \\ 0 \end{bmatrix}$ is the input matrix. The vector $x(t) \in \mathbb{R}^{2\times 1}$ is the state vector. The matched disturbance $\delta(x(t), t))$ on the system is a combination of the wing rock dynamics $\delta_{wr}(x(t))$ and external disturbance $\delta_{ex}(t)$.

$$\delta(x(t), t)) = \delta_{wr}(x(t)) + \delta_{ex}(t) \tag{2.3}$$

The wing rock dynamics is defined in [53] by

$$\delta_{wr}(x(t)) = \alpha_1 x_2 + \alpha_2 x_1 + \alpha_3 |x_2| x_1 + \alpha_4 |x_1| x_1 + \alpha_5 x_1^3. \tag{2.4}$$

The equation representing wing rock dynamics is in a form that constant aerodynamic coefficients are multiplied with nonlinear functions of the system states. The numerical values of the aerodynamic coefficients of the wing rock are $\alpha_1 = 0.1414$, $\alpha_2 = 0.5504$, $\alpha_3 = -0.0624$, $\alpha_4 = 0.0095$, and $\alpha_5 = 0.0215$ as selected in [66]. The

wing rock dynamics equation can be rewritten in vector form as follows

$$\begin{aligned}\delta_{wr}\left(x(t)\right) &= \begin{bmatrix} \alpha_1 & \alpha_2 & \alpha_3 & \alpha_4 & \alpha_5 \end{bmatrix} \begin{bmatrix} x_2 \\ x_1 \\ |x_2|x_1 \\ |x_1|x_1 \\ x_1^3 \end{bmatrix} \\ &= \alpha f\left(x(t)\right)\end{aligned} \tag{2.5}$$

with $\alpha \in \mathbb{R}^{1\times 5}$ and $f\left(x(t)\right) \in \mathbb{R}^{5\times 1}$.

The external disturbance ($\delta_{ex}(t)$) is a random disturbance which is function of time. This disturbance is included to the system in order to represent the wind and gust effects that occur randomly on the air. By this addition, the system model has three main components. The first component is the linear system model which is assumed to be known. The second component is the wing rock dynamics formed by multiplication of known functions of system states and unknown constant aerodynamic coefficients, and the third component is totally unknown random disturbance which is a function of time. The block diagram for the sample system model is shown in the Figure 2.1.

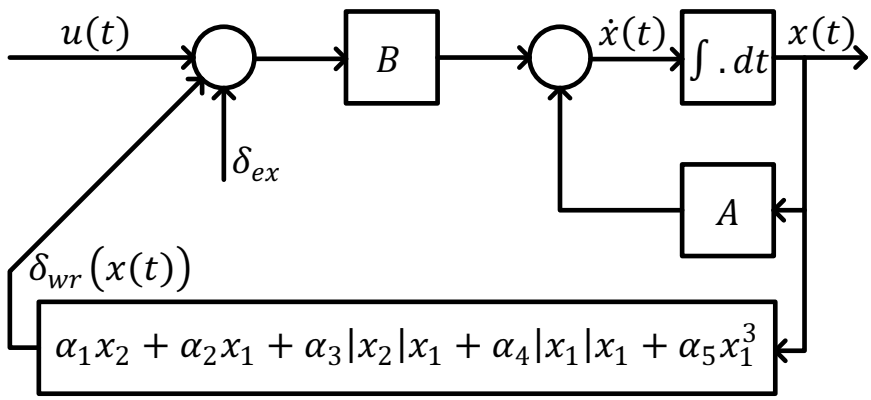

Figure 2.1: System model block diagram.

Another physical system need to be modeled is the control actuator system. The control actuator system shows the dynamics between the commanded control input and the actuated control input of the system. For the modeling of the control actuator system, a second order linear differential equation is used. This equation is

$$\dot{x}_c = A_c x_c(t) + B_c u_c(t) \tag{2.6}$$

where $x_c(t) \in \mathbb{R}^{2\times 1}$ is the state vector of control actuator system, and $u_c(t) \in \mathbb{R}$ is the commanded input to the system. The state vector is formed by the actuated control input $u(t)$ and its derivative $\dot{u}(t)$, $x_c(t) = \begin{bmatrix} u(t) \\ \dot{u}(t) \end{bmatrix}$. $A = \begin{bmatrix} 0 & 1 \\ -\omega_c^2 & -2\zeta_c\omega_c \end{bmatrix}$ is the system matrix of the control actuator system, and $B = \begin{bmatrix} 0 \\ \omega_c^2 \end{bmatrix}$ is the input matrix. The natural frequency of the control actuator system is shown by ω_c and the damping ratio is ζ_c. The control actuator model for the system used in this study is selected with $\omega_c = 50\ rad/s$ and $\zeta_c = 0.7$.

The system and control actuator model can be combined as,

$$\begin{bmatrix} \dot{x}_1(t) \\ \dot{x}_2(t) \\ \dot{u}(t) \\ \ddot{u}(t) \end{bmatrix} = \begin{bmatrix} 0 & 0 & 1 & 0 \\ 1 & 0 & 0 & 0 \\ 0 & 0 & 0 & 1 \\ 0 & 0 & -\omega_c^2 & -2\zeta_c\omega_c \end{bmatrix} \begin{bmatrix} x_1(t) \\ x_2(t) \\ u(t) \\ \dot{u}(t) \end{bmatrix} + \begin{bmatrix} 0 \\ 0 \\ 0 \\ \omega_c^2 \end{bmatrix} u_c(t) + \begin{bmatrix} 1 \\ 0 \\ 0 \\ 0 \end{bmatrix} \delta\left(x(t), t\right). \quad (2.7)$$

This combined system equation can be rewritten in shorter form as

$$\dot{x}_p(t) = A_p x_p(t) + B_p u_c(t) + B_d \delta\left(x(t), t\right) \quad (2.8)$$

where $A_p \in \mathbb{R}^{4\times 4}$ is the plant system matrix, $B_p \in \mathbb{R}^{4\times 1}$ is the plant input matrix, and $B_d \in \mathbb{R}^{4\times 1}$ is the disturbance input matrix.

The controllability of the combined system shown in (2.8) can be examined by the rank of the controllability matrix

$$\mathcal{C} = \begin{bmatrix} B_p & A_p B_p & A_p^2 B_p & A_p^3 B_p \end{bmatrix}. \quad (2.9)$$

Since the controllability matrix $\mathcal{C} \in \mathbb{R}^{4\times 4}$ is full rank, the combined system is controllable.

2.2 Design of Model Following Control

The system model representing the system dynamics is obtained. The next step for the MFC design is the selection of the reference model. The selection starts with the desired natural frequency ω_n and damping ratio ζ_n. These criteria for the system transient response form the desired dynamics of the reference model.

The reference model can be selected directly as a second order differential equation with desired natural frequency and damping ratio; however, it is preferred to select the reference model using the system model. The system model is shown to be controllable; so, the eigenvalues of the system model can be placed at desired locations with the use of a full state feedback method. The gain calculation for the full state feedback is done using the Ackermann's formula [42].

The plant model shown in (2.8) has four states. These states are roll rate, roll angle, actuated control input and its derivative. In spite of this, there are only two desired criteria for design. Therefore, eigenvalues of the two states regarding the control actuator system are kept at their original position and the eigenvalues of the other two states regarding the rigid body motion of the system are placed at the desired locations.

The desired locations for the eigenvalues are calculated from the roots of the characteristic equation of the desired dynamics

$$s^2 + 2\zeta_n\omega_n s + \omega_n^2 = 0. \tag{2.10}$$

These roots are $\lambda_1 = -\zeta_n\omega_n + \sqrt{\zeta_n^2\omega_n^2 - \omega_n^2}$ and $\lambda_2 = -\zeta_n\omega_n - \sqrt{\zeta_n^2\omega_n^2 - \omega_n^2}$. Similarly, roots of the control actuator system are $\lambda_3 = -\zeta_c\omega_c + \sqrt{\zeta_c^2\omega_c^2 - \omega_c^2}$ and $\lambda_4 = -\zeta_c\omega_c - \sqrt{\zeta_c^2\omega_c^2 - \omega_c^2}$. Roots of the two characteristic equations are the desired eigenvalues for the reference model. Therefore, the characteristic equation of the reference model should be in the form

$$(s - \lambda_1)(s - \lambda_2)(s - \lambda_3)(s - \lambda_4) = 0. \tag{2.11}$$

This condition can be satisfied by using the Ackermann's formula as mentioned before. Ackermann's formula is used to calculated the necessary full state feedback gains for a system to have the desired characteristic equation. This formula for a forth order system can be shown as

$$K_r = \begin{bmatrix} 0 & 0 & 0 & 1 \end{bmatrix} \mathcal{C}(A_p - \lambda_1 I_{4\times4})(A_p - \lambda_2 I_{4\times4})(A_p - \lambda_3 I_{4\times4})(A_p - \lambda_4 I_{4\times4}). \tag{2.12}$$

The matrix $\mathcal{C}$ is the controllability matrix shown in (2.9), and $I_{4\times4} \in \mathbb{R}^{4\times4}$ is the identity matrix. The calculated gain vector $K_r \in \mathbb{R}^{1\times4}$ is the feedback gain vector to

obtain the reference model dynamics. The equation regarding the reference model is

$$\begin{aligned}\dot{x}_r(t) &= (A_p - B_p K_r)x_r(t) + B_p K_r \begin{bmatrix} 0 \\ 1 \\ 0 \\ 0 \end{bmatrix} r(t) \\ &= A_r x_r(t) + B_r r(t).\end{aligned} \tag{2.13}$$

The system matrix of the reference model is $A_r \in \mathbb{R}^{4\times 4}$, and the input matrix is $B_r \in \mathbb{R}^{4\times 1}$. The state vector of the reference model is $x_r(t) \in \mathbb{R}^{4\times 1}$, and the reference command is $r(t) \in \mathbb{R}$.

The desired natural frequency and damping ratio for the reference model are selected as $\omega_n = 0.4\, rad/s$ and $\zeta_n = 0.707$. The reference model controller gain is calculated by the Ackermann's formula as $K_r = \begin{bmatrix} 0.57 & 0.16 & 0 & 0 \end{bmatrix}$. The last two gains in the reference model controller gain vector are equal to zero; since, last two states of the system are wanted to protect their open-loop responses. These states are the controller actuator states and the eigenvalues regarding these states are kept in the original positions. The step response of the reference model is shown in the Figure 2.2.

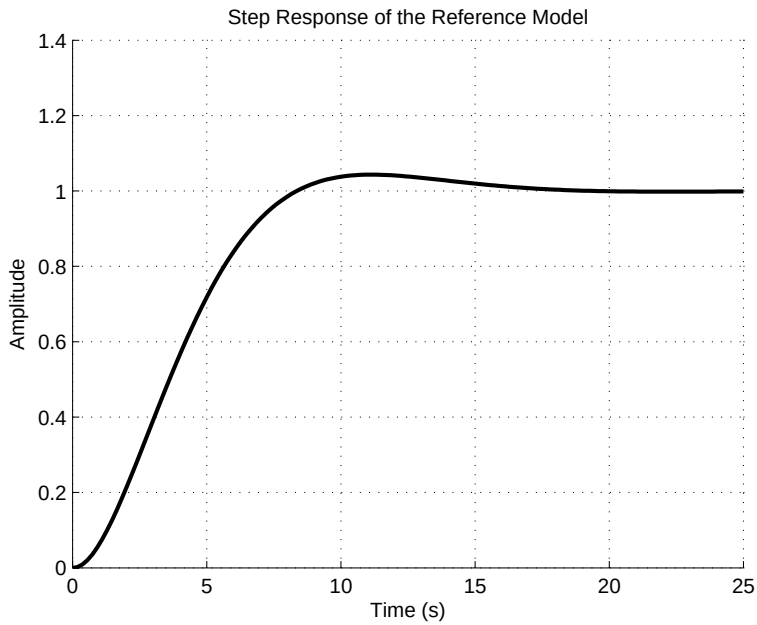

Figure 2.2: Step response of the reference model.

The desired response of the system is defined by the reference model, so, the step response shown in Figure 2.2 is also the desired response of the closed-loop system.

The plant dynamics equation (2.8) and the reference model equation (2.13) can be combined as

$$\dot{x}_{pr}(t) = \begin{bmatrix} \dot{x}_p(t) \\ \dot{x}_r(t) \end{bmatrix} = \begin{bmatrix} A_p & 0_{4\times4} \\ 0_{4\times4} & A_r \end{bmatrix} x_{pr}(t) + \begin{bmatrix} B_p \\ 0_{4\times1} \end{bmatrix} u_c(t) + \begin{bmatrix} 0_{4\times1} \\ B_r \end{bmatrix} r(t). \quad (2.14)$$

The state vector of the combined equation above is $x_{pr} \in \mathbb{R}^{8\times1}$. This equation can be rewritten in more compact form as

$$\dot{x}_{pr}(t) = A_{pr}x_{pr}(t) + B_{pru}u_c(t) + B_{prr}r(t). \quad (2.15)$$

The system matrix of the combined system is $A_{pr} \in \mathbb{R}^{8\times8}$, the control input matrix is $B_{pru} \in \mathbb{R}^{8\times1}$, and the reference command input matrix is $B_{prr} \in \mathbb{R}^{8\times1}$.

The integral of the error between the plant roll angle and the reference roll angle is added to the system as an integral state. This integral state is calculated with the given equation

$$\dot{x}_i(t) = \begin{bmatrix} 0 & -1 & 0_{1\times3} & 1 & 0_{1\times2} \end{bmatrix} x_{pr} = x_{r2} - x_2. \quad (2.16)$$

The integral state itself is

$$x_i = \int_{t=0}^{t} (x_{r2} - x_2)dt. \quad (2.17)$$

Here the state x_2 is the roll angle of the system as shown in (2.1), and the state x_{r2} is the second state in the state vector of the reference model dynamics equation shown in (2.13) which corresponds to the reference value of the roll angle.

The integral state is added to the combined equation shown in (2.14) as

$$\dot{x}_s = \begin{bmatrix} \dot{x}_{pr} \\ \dot{x}_i \end{bmatrix} = \begin{bmatrix} A_{pr} & & & & & 0_{8\times1} \\ 0 & -1 & 0_{1\times3} & 1 & 0_{1\times2} & 0 \end{bmatrix} \begin{bmatrix} x_{pr} \\ x_i \end{bmatrix} + \begin{bmatrix} B_{pru} \\ 0 \end{bmatrix} u_c(t) + \begin{bmatrix} B_{prr} \\ 0 \end{bmatrix} r(t). \quad (2.18)$$

This equation is the open-loop equation of the total system for the design of MFC. Equation (2.18) can be rewritten in compact form as

$$\dot{x}_s = A_o x_s + B_{ou}u_c(t) + B_{or}r(t) \quad (2.19)$$

where, $x_s \in \mathbb{R}^{9\times1}$ is the state vector, $A_0 \in \mathbb{R}^{9\times9}$ is the system matrix, $B_{ou} \in \mathbb{R}^{9\times1}$ is the control input matrix, and $B_{or} \in \mathbb{R}^{9\times1}$ is the reference command input matrix of the open loop system equation.

The open-loop system equation is formed mathematically in (2.19). The states of this open-loop model are roll rate $x_1(t)$, roll angle $x_2(t)$, actuated control input $u(t)$,

derivative of the actuated control input $\dot{u}(t)$, reference roll rate $x_{r1}(t)$, reference roll angle $x_{r2}(t)$, reference actuated control input $x_{r3}(t)$, derivative of the reference actuated control input $x_{r4}(t)$, and error integral $x_i(t)$. Among these only the first four are physical states. The other five of them are synthetic states that are calculated inside the control computer. With this information and with the assumption of the physical states can be measured, all of the states of the open-loop system equation are available for feedback.

The feedback gain of the MFC is calculated optimally. The optimality is obtained by minimization of a cost function. The selected cost function to be minimized is quadratic in performance vector. The performance vector is formed by the linear combination of the selected system states and control inputs. For this problem, the performance vector is selected as

$$z(t) = \begin{bmatrix} (x_{r1} - x_1) & (x_{r2} - x_2) & (x_{r3} - u) & (x_{r4} - \dot{u}) & x_i & u_c \end{bmatrix}^T \tag{2.20}$$

with $z \in \mathbb{R}^{6\times 1}$. The linear combination of the states included in the performance vector are penalized by selected weightings. The weight matrix is in the form $Q_z = diag\left(\begin{bmatrix} Q_{x_1} & Q_{x_2} & Q_u & Q_{\dot{u}} & Q_{x_i} & Q_{u_c} \end{bmatrix}\right) \in \mathbb{R}^{6\times 6}$. The cost function to be minimized for obtaining the optimal controller gain is

$$J = \int_{t=0}^{\infty} (z^T(t) Q_z z(t)) dt. \tag{2.21}$$

This cost function can be transformed to the well known linear quadratic regulation cost function;

$$J = \int_{t=0}^{\infty} \left(x_s^T(t) W_x x_s(t) + u_c^T(t) W_u u_c(t) + 2 x_s^T(t) W_{xu} u_c(t) \right) dt. \tag{2.22}$$

The performance vector $z(t)$ is formed with the following relation

$$z(t) = C_z x_s(t) + D_z u_c(t) \tag{2.23}$$

where $C_z = \begin{bmatrix} -I_{4\times 4} & I_{4\times 4} & 0_{4\times 1} \\ 0_{1\times 4} & 0_{1\times 4} & 1 \\ 0_{1\times 4} & 0_{1\times 4} & 0 \end{bmatrix} \in \mathbb{R}^{6\times 9}$ is the selector matrix from the system states, and $D_z = \begin{bmatrix} 0_{5\times 1} \\ 1 \end{bmatrix} \in \mathbb{R}^{6\times 1}$ is the selector matrix from the system commanded control input. By inserting (2.23) into (2.21), the cost function equation can

be rewritten as

$$J = \int_{t=0}^{\infty} \Big(\left(C_z x_s(t) + D_z u_c(t)\right)^T Q_z \left(C_z x_s(t) + D_z u_c(t)\right) \Big) \, dt \tag{2.24}$$

which yields

$$J = \int_{t=0}^{\infty} \left(\left(x_s^T(t) C_z^T Q_z + u_c^T(t) D_z^T Q_z\right) \left(C_z x_s(t) + D_z u_c(t)\right) \right) dt. \tag{2.25}$$

Furthermore, the terms can be collected as

$$J = \int_{t=0}^{\infty} \left(x_s^T(t) C_z^T Q_z C_z x_s(t) + u_c^T(t) D_z^T Q_z D_z u_c(t) + 2 x_s^T(t) C_z^T Q_z D_z u_c(t) \right) dt. \tag{2.26}$$

By comparing the equivalent terms in (2.22) and (2.26), the relation between the weight matrices can be found as

$$W_x = C_z^T Q_z C_z \quad W_u = D_z^T Q_z D_z \quad W_{xu} = C_z^T Q_z D_z \tag{2.27}$$

where $W_x \in \mathbb{R}^{9\times 9}$, $W_u \in \mathbb{R}$ and $W_{xu} \in \mathbb{R}^{9\times 1}$.

The optimal solution for the minimization of the cost function with the control law

$$u_c(t) = -K x_s(t), \tag{2.28}$$

gives the total gain $K \in \mathbb{R}^{1\times 9}$ of the MFC. The resulting controller gain K is calculated by using the well known linear quadratic regulation method. For this method, first the Riccati equation

$$A_o^T X + X A_o - (X B_{ou} + W_{xu}) W_u^- 1 (B_{ou}^T X + W_{xu}^T) + W_x \tag{2.29}$$

is solved. Here, $X \in \mathbb{R}^{9\times 9}$ is the solution of the Riccati equation. Then, the controller gain is calculated with the relation

$$K = W_u^- 1 (B_{ou}^T X + N^T). \tag{2.30}$$

So, the design is concluded.

The closed-loop equation for the MFC is found by replacing the commanded control input with (2.28) as

$$\begin{aligned} \dot{x}_s(t) &= A_o x_s(t) + B_{ou} \left(-K x_s(t)\right) + B_{or} r(t) \\ &= \left(A_o - B_{ou} K\right) x_s(t) + B_{or} r(t) \\ &= A_{cl} x_s(t) + B_{cl} r(t). \end{aligned} \tag{2.31}$$

The closed-loop system matrix is $A_{cl} \in \mathbb{R}^{9\times 9}$, and the closed-loop input matrix is $B_{cl} \in \mathbb{R}^{9\times 1}$.

The block diagram of the MFC is shown in the Figure 2.3. As it can be seen from the figure, the reference model is directly driven by the reference command, and the combined state vector is multiplied with the controller gain K in order to calculate the commanded control input u_c.

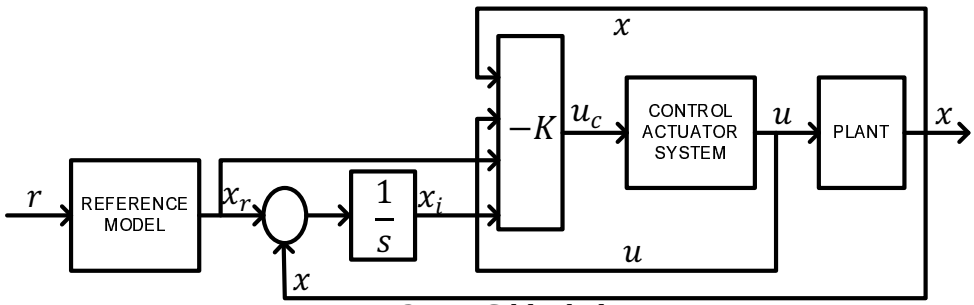

Figure 2.3: MFC block diagram.

For the given desired reference model criteria, the weight matrix Q_z is selected as

$$Q_z = \begin{bmatrix} 0.1 & 0 & 0 & 0 & 0 & 0 \\ 0 & 100 & 0 & 0 & 0 & 0 \\ 0 & 0 & 1 & 0 & 0 & 0 \\ 0 & 0 & 0 & 1 & 0 & 0 \\ 0 & 0 & 0 & 0 & 1000 & 0 \\ 0 & 0 & 0 & 0 & 0 & 1 \end{bmatrix}. \tag{2.32}$$

The selection of the Q_z is done by searching the weights while examining the time domain response and robustness properties of the designed controller. These properties will be discussed in the following sections.

The resulting controller gain K is

$$K = \begin{bmatrix} 20.9 & 37.7 & 5.6 & 1 & -20.9 & -37.7 & -5.6 & -1 & -31.6 \end{bmatrix}. \tag{2.33}$$

The design of the MFC for the sample system is concluded with the calculation of the controller gain K.

2.3 Robustness Analysis

Robustness analysis of the MFC method is composed of two analyses. The first one is the disturbance rejection analysis, where the effect of the disturbances on the system are examined in the frequency domain. And the second one is the noise filtering analysis. In this analysis, the noise rejection performance of the controller is examined.

2.3.1 Disturbance Rejection

The disturbance acting on the system model is defined in (2.3) as $\delta\left(x(t), t\right)$. In order to examine the effect of the disturbance on the system, other inputs such as reference command and noise are equaled to zero. Since the only input on the system is the disturbance, transfer function from the disturbance to the roll angle can be calculated. This transfer function gives the opportunity to examine the frequency domain characteristic of disturbance rejection of the MFC.

The states of the reference model are kept zero under zero reference command and zero initial conditions. Therefore, for the disturbance rejection analysis, the reference model is ineffective. But the optimal controller design is done using the dynamics of the reference model, so, the reference model is still affecting the disturbance rejection performance via the controller gains.

The block diagram of the MFC with disturbance $\delta\left(x(t), t\right)$ acting on the system is shown in the Figure 2.4.

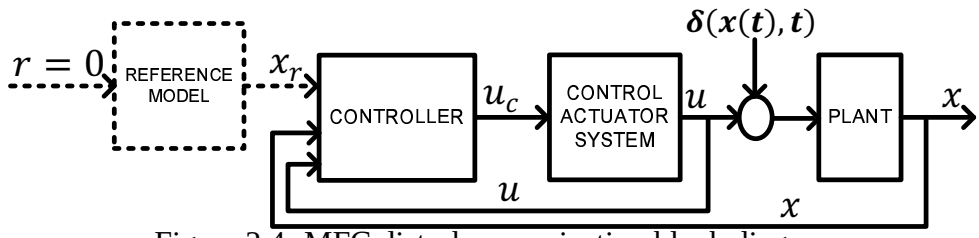

Figure 2.4: MFC disturbance rejection block diagram.

In order to examine the disturbance rejection performance of the MFC, the transfer function from the disturbance δ to the roll angle x_2 is evaluated. The combined system

equation given in (2.8) can be written in transfer function form with $x_r = 0_{4\times1}$ as

$$sx_p = A_p x_p - B_p K \begin{bmatrix} x_p \\ 0_{4\times1} \\ \frac{1}{s}\left(-C_{x_2} x_p\right) \end{bmatrix} + B_d \delta. \tag{2.34}$$

where $C_{x_2} = \begin{bmatrix} 0 & 1 & 0_{1\times2} \end{bmatrix}$. The selection matrix C_{x_2} is used to select the roll angle from the plant states x_p. The terms containing the state vector of the plant x_p can be grouped together as

$$\left(sI_{4\times4} - A_p + B_p K \begin{bmatrix} I_{4\times4} \\ 0_{4\times4} \\ \frac{1}{s}\left(-C_{x_2} I_{4\times4}\right) \end{bmatrix} \right) x_p = B_d \delta. \tag{2.35}$$

The plant state vector x_p can be left alone by taking the inverse of the terms in the big parenthesis which is $A_{ps} = \left(sI_{4\times4} - A_p + B_p K \begin{bmatrix} I_{4\times4} \\ 0_{4\times4} \\ \frac{1}{s}\left(-C_{x_2} I_{4\times4}\right) \end{bmatrix} \right)$. With this replacement, (2.35) can be rewritten as

$$x_p = A_{ps}^{-1} B_d \delta. \tag{2.36}$$

The roll angle can be selected from the plant state vector with the relation shown as

$$x_2 = C_{x_2} x_p. \tag{2.37}$$

So, the transfer function from the disturbance δ to the roll angle x_2 is calculated as

$$\frac{x_2}{\delta}(s) = C_{x_2} A_{ps}^{-1} B_d. \tag{2.38}$$

The numerical disturbance rejection transfer function for the designed MFC is

$$\frac{x_2}{\delta}(s) = \frac{s^3 + 2507s^2 + 1.66\ 10^4 s}{s^5 + 2507s^4 + 1.66\ 10^4 s^3 + 5.22\ 10^4 s^2 + 9.42\ 10^4 s + 7.91\ 10^4}. \tag{2.39}$$

The magnitude plot of the disturbance rejection transfer function of MFC is shown in the Figure 2.5.

The magnitude change shown in the Figure 2.5 displays the disturbance rejection performance of the MFC design. This magnitude plot gives proportional information

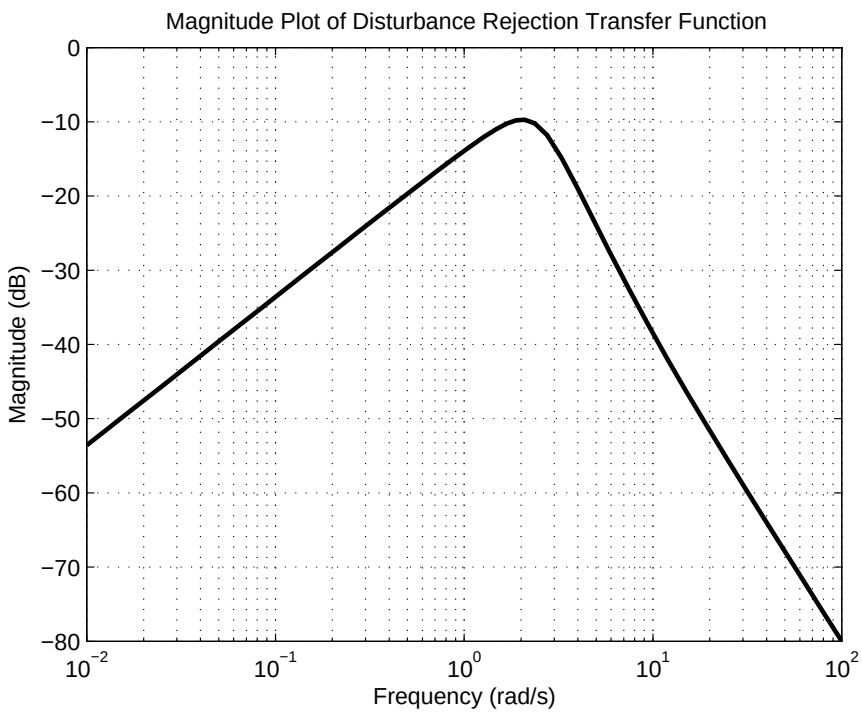

Figure 2.5: Magnitude plot of disturbance rejection transfer function.

about how a disturbance acting on the system could be suppressed by the controller. For a selected frequency in the Figure 2.5, the corresponding magnitude shows the ratio of the size of the disturbance to its effect on the roll angle. The peak response of the diagram appears at $2.1 rad/s$. At this frequency, the controller conducts the disturbance most with a multiplier of $-9.7\,dB$. This is equivalent to a ratio of 0.33 between the magnitude of the disturbance and the effect on the roll angle. This frequency is the peak frequency of the magnitude plot of disturbance rejection transfer function. Therefore, for the designed controller, the most effective disturbance can occur at $2.1\ rad/s$. The disturbance rejection magnitude plot has a slope of $-20\ dB/decade$ below the peak frequency and has a slope of $-40\ dB/decade$ above the peak frequency. So, the robustness to disturbance increases for disturbances with lower and higher frequencies then the peak frequency.

The robustness to disturbance is one of the criteria that is used in the selection of the weighting matrix for the performance vector (2.32). In addition to this criterion, there are more robustness and performance based criteria for the design.

The robustness of the MFC method is shown to be better than some classical and optimal controllers widely used in the literature [18].

2.3.2 Noise Filtering

Measurement devices are used to measure certain information regarding the states of the system. For example, a gyroscope measures the turn rate of the system. The output of the measurement device includes both the turn rate information and some meaningless oscillations. These meaningless oscillations are called the noise on the measurement. These noisy measurements are used as feedback to the controller. By this way, the noise acts on the system.

In order to control the system properly and calculate smooth control commands, a controller needs the noise on the feedback to be filtered. The noise filtering robustness character plays its role in this stage. A good noise filtering character results a smoother control command. The noise filtering character of a controller is examined by the transfer function between the noise input to the roll angle output of the system.

For the MFC all of the physical states of the sample system model shown in (2.7) are assumed to be available. The synthetic states added to the system by the reference model and the integrator shown in the combined system equation (2.18) are also available for feedback since they are calculated inside the controller.

For the physical system states, the first state corresponds to the roll rate $x_1(t)$. The roll rate is measured by the gyroscope and noise due to this measurement is added to the system by the measurement device. The second state is the roll angle $x_2(t)$. The roll angle is calculated by integrating the roll rate, so this state does not introduce any additional noise into the system. The other two states are the control actuator states ($u(t), \dot{u}(t)$). The controller angle is measured by the encoder. The encoder measurement device is an absolute device so the noise it introduces in the system feedback is neglected in this study. Similarly, the noise introduced on the system due to derivation of the encoder output is also neglected. Therefore, for the physical states of the sample system, noise is only introduced on the roll rate measurement. This noise is called as the noise on the first state of the system $n_{x_1}(t)$, and it is a random oscillation with time.

For the synthetic states calculated in the controller, the possible noise occurring due to computation is also neglected. Therefore, the only noise on the system is $n_{x_1}(t)$.

The block diagram with the noise input to the system is shown in the Figure 2.6.

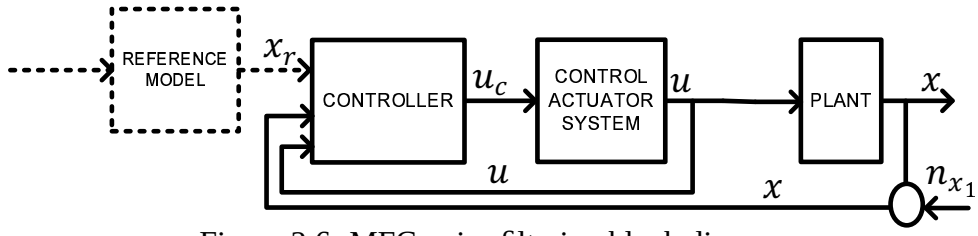

Figure 2.6: MFC noise filtering block diagram.

The open-loop system equation shown in (2.19) is

$$\dot{x}_s = A_o x_s + B_{ou} u_c(t) + B_{or} r(t). \tag{2.40}$$

The control deflection command calculation equation (2.28) is updated with the noise input to the system as

$$u_c(t) = -K \begin{bmatrix} x_1(t) + n_{x_1}(t) \\ x_2(t) + \int (n_{x_1}(t) dt) \\ u(t) \\ \dot{u}(t) \\ x_{r1}(t) \\ x_{r2}(t) \\ x_{r3}(t) \\ x_{r4}(t) \\ x_i(t) \end{bmatrix}. \tag{2.41}$$

The reference command $r(t)$ and the disturbance on the system $\delta\left(x(t), t\right)$ shown in the Figure 2.4 are assumed to be zero. This assumption is done in order to satisfy the single input single output form of the plant. The only input to the system is the roll rate measurement noise $n_{x_1}(t)$, and the output is taken as the roll angle $x_2(t)$.

The system equation with the above assumptions is

$$\dot{x}_s = A_o x_s - B_{ou} K \begin{bmatrix} x_1(t) + n_{x_1}(t) \\ x_2(t) + \int (n_{x_1}(t) dt) \\ u(t) \\ \dot{u}(t) \\ x_{r1}(t) \\ x_{r2}(t) \\ x_{r3}(t) \\ x_{r4}(t) \\ x_i(t) \end{bmatrix}. \tag{2.42}$$

Equation (2.42) can be rewritten in transfer function form by using the relations; $\dot{()}$ is s, and $\int () dt$ is $\frac{1}{s}$. The system states and the noise input can be separated and the equation can be rewritten as

$$s x_s = A_o x_s - B_{ou} K x_s - B_{ou} K \begin{bmatrix} 1 \\ \frac{1}{s} \\ 0_{7\times1} \end{bmatrix} n_{x_1}. \tag{2.43}$$

Collecting the input n_{x_1} and the states x_s in separate parts gives

$$(s I_{9\times9} - A_o + B_{ou} K) x_s = -B_{ou} K \begin{bmatrix} 1 \\ \frac{1}{s} \\ 0_{7\times1} \end{bmatrix} n_{x_1}. \tag{2.44}$$

The roll angle x_2 can be selected from the system states with the following relation

$$x_2 = C_{x_{s2}} x_s. \tag{2.45}$$

The x_2 selection matrix is $C_{x_{s2}} = \begin{bmatrix} 0 & 1 & 0_{1\times7} \end{bmatrix}$. By using the relations shown in (2.44) and (2.45), the noise filtering transfer function from noise n_{x_1} to roll angle x_2 is found as

$$\frac{x_2}{n_{x_1}}(s) = -C_{x_{s2}} (s I_{9\times9} - A_o + B_{ou} K)^{-1} B_{ou} K \begin{bmatrix} 1 \\ \frac{1}{s} \\ 0_{7\times1} \end{bmatrix}. \tag{2.46}$$

The numerical transfer function calculated for the designed controller is

$$\frac{x_2}{n_{x_1}}(s) = \frac{-5.22\,10^4 s - 9.42\,10^4}{s^5 + 2507s^4 + 1.66\,10^4 s^3 + 5.22\,10^4 s^2 + 9.42\,10^4 s + 7.91\,10^4}. \quad (2.47)$$

The noise filtering character of the MFC is examined by using the noise filtering transfer function. The magnitude plot of the noise filtering transfer function (2.47) is shown in the Figure 2.7.

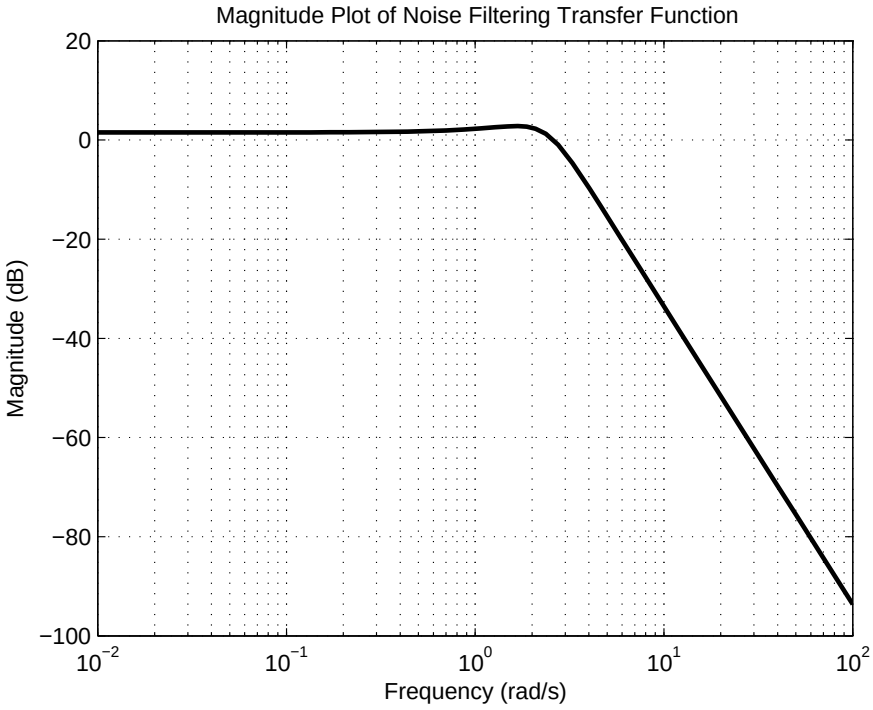

Figure 2.7: Magnitude plot of noise filtering transfer function.

The magnitude plot of the noise filtering transfer function shows the effect of noise on the roll angle. For different frequencies, the augmented system with controller passes the noise in different levels. By examining the Figure 2.7 it can easily be seen that noise filtering performance of the controller increases as the frequency of the noise increases. Since random noises oscillation occur on high frequencies, this character is a good noise filtering character. The peak of the noise pass occurs at $1.6\,rad/s$ frequency. The magnitude of the multiplier at the peak point is $2.8\,dB$. For the frequencies below of the peak frequency, the noise pass has an almost constant magnitude. The magnitude value for the low frequencies is around $1.5\,dB$. This value wanted to be lower for better noise filtering, but for the low frequency regime this value is acceptable since most of the noise occurs on high frequencies. For the frequencies higher than the peak frequency, the magnitude plot has a slope of $-60\,dB/decade$.

This means for every tenth power of frequency the noise is suppressed $60\ dB$ more. Therefore, as the frequency of the noise increases, the noise filtering effect on the measurement gets stronger.

2.4 Simulation Examples

The performance and the robustness of the designed controller is examined by simulations. The plant model for the slender delta wing combined with the control actuator model and disturbance input is given in (2.7). The disturbance acting on the system is composed of two parts as mentioned in 2.1. The first part of the disturbance is the wing rock dynamics. The wing rock dynamics introduce external moment on the system for roll angle and roll rates of the delta wing. The mathematical relation between states of the system and the wing disturbance $\delta_{wr}\left(x(t)\right)$ is given in (2.4) and can be repeated as

$$\delta_{wr}(x(t)) = \alpha_1 x_2 + \alpha_2 x_1 + \alpha_3 |x_2| x_1 + \alpha_4 |x_1| x_1 + \alpha_5 x_1^3. \tag{2.48}$$

The second part of the disturbance acting on the system is the random external disturbance. The random external disturbance $\delta_{ex}\left(t\right)$ acting on the system is neglected in this section and is going to be taken into account in the following section 2.5. So the numerical details are also going to be mentioned in the following section.

The noise acting on the measurement of the system roll rate $n_{x_1}(t)$ is assumed as a Gaussian distributed random signal with zero mean and $1\ 10^{-}4\ rad/s$ variance.

The measurement device dynamics are neglected since the system's bandwidth is relatively lower than most of the gyroscope devices used for measuring the roll rate. Therefore, the roll rate information is assumed to be measured without lag. However, the noise introducing effect of the device is kept in the simulations.

The block diagram of the system with the wing rock dynamics, external disturbance and measurement noise inputs is shown in the Figure 2.8.

Two different reference command set is applied for the performance inspection of the MFC controller. The first one is a step sequence and the second one is a sine wave. The results of the simulations are shown in 2.4.1 and 2.4.2.

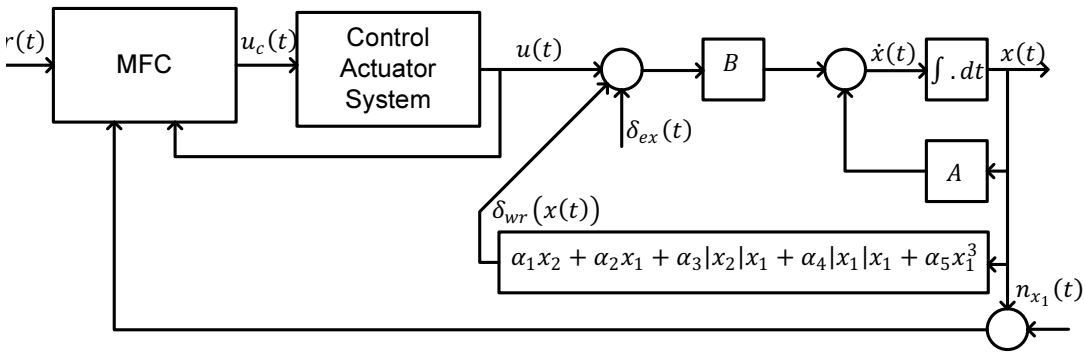

Figure 2.8: MFC block diagram for simulation.

2.4.1 Step Command

The reference input to the system controlled with MFC is selected as a step sequence. The magnitudes of the steps are $\pm 5\ deg$ with a period of $50\ secs$. The plot of the step command is shown in the Figure 2.9.

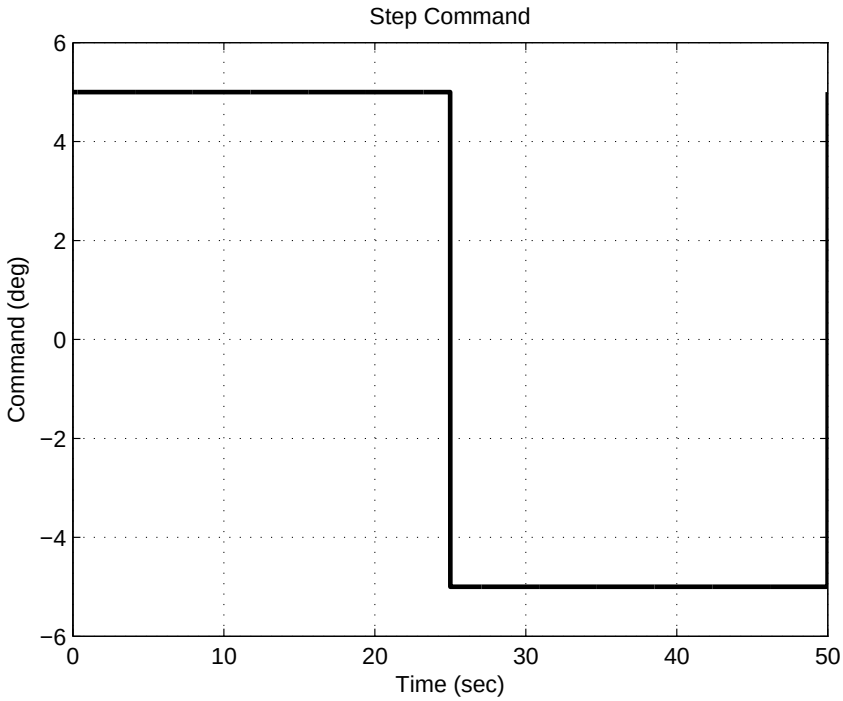

Figure 2.9: Step command input.

In order to examine the performance of the controller, three different simulations are done for the given step command. First, the both the disturbances and noise input is closed. The block diagram of the system for the first simulation of the step command is shown in the Figure 2.10.

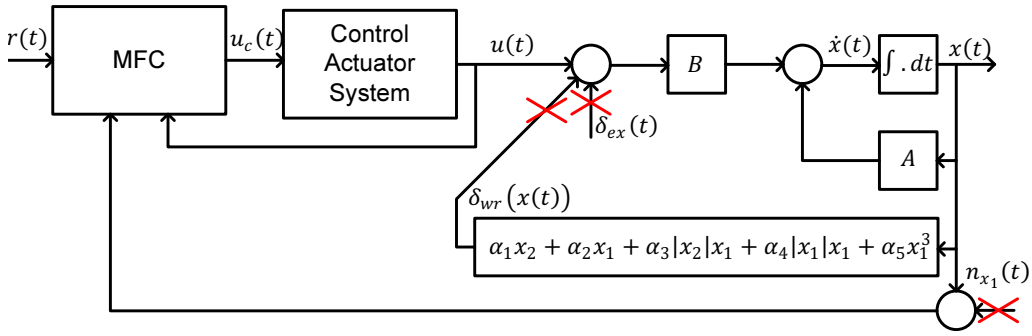

Figure 2.10: MFC block diagram with no disturbance and noise.

The step stair command, the response of the reference model, and the response of the controller are shown in the Figure 2.11.

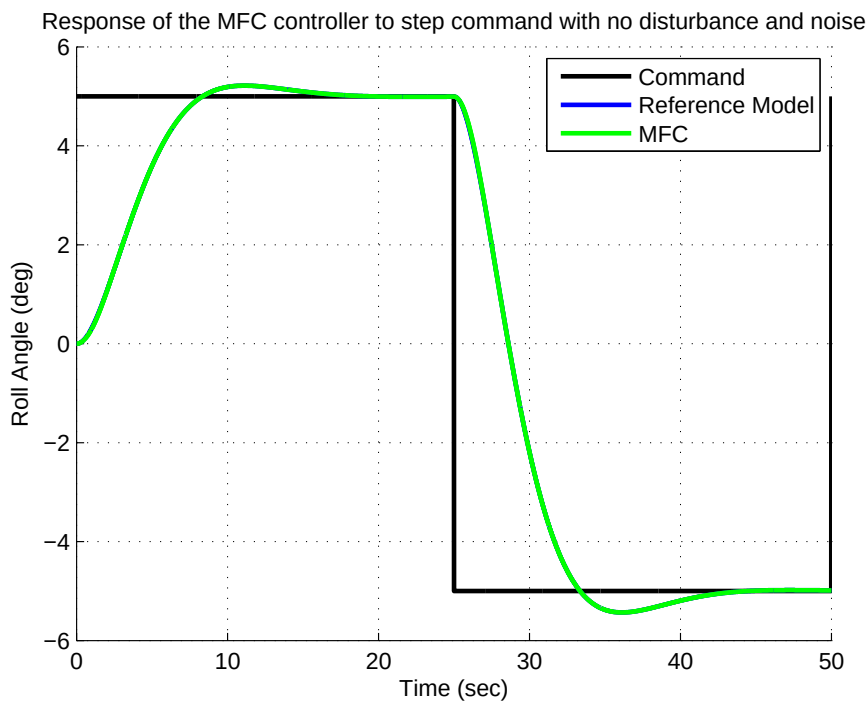

Figure 2.11: MFC response with no disturbance and noise.

In the figure, the black line corresponds to the stair step command input to the system. The blue line, which can not be seen, since it is hided under the green line; is corresponds to the roll angle of the reference model. The green line is the roll angle of the slender delta wing, which is obtained by using the MFC.

As it can be seen from the Figure 2.11, the controller can follow the reference model perfectly where there are no disturbance and noise introduced to the system. This result is an expected result and shows that the controller design is done accurately.

In the next simulation with step command, the disturbance due to the wing rock dynamics $\delta_{wr}\left(x(t)\right)$ is introduced. This dynamics is defined in (2.48) and are nonlinear dynamics. The block diagram used for the second simulation is shown in the Figure 2.12

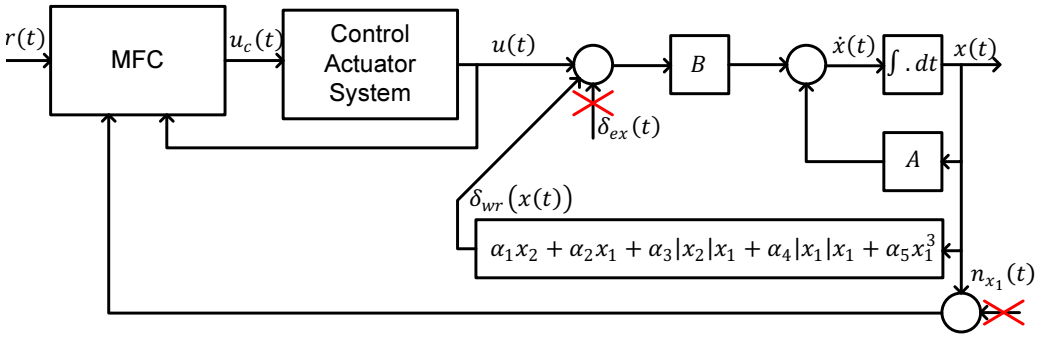

Figure 2.12: MFC block diagram with wing rock dynamics.

The response of the controller for the step command, while the wing rock dynamics are acting to the system, is shown in the Figure 2.13.

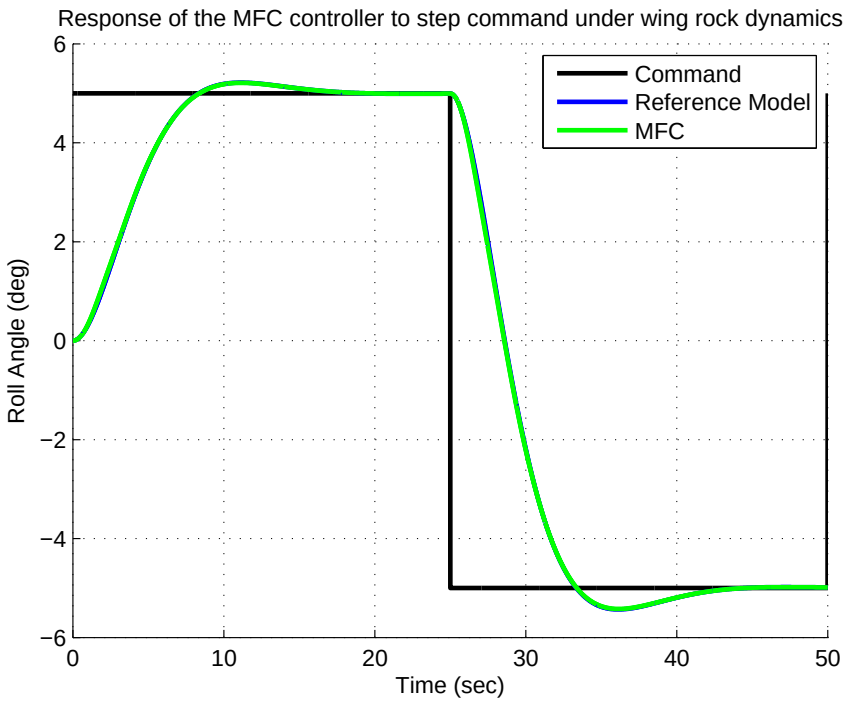

Figure 2.13: MFC response to step command under the effect of wing rock dynamics.

The MFC is designed for being robust to the disturbances. This character of the controller is examined in the section 2.3. The magnitude plot of the disturbance rejection transfer function, which can be examined in the Figure 2.5, shows how effectively the MFC can suppress disturbances acting on the system. This character

of the controller also can be seen from the Figure 2.13. In this figure, the response of the system, which is shown by the green line, has a really close tracking performance of the reference roll angle, which is shown by the blue line. For the defined wing rock dynamics, which is taken from [53, 66], the MFC is shown to have satisfactory disturbance rejection performance while following a stair step command.

Since the optimal model following controller is shown to have a fulfilling disturbance rejection performance, the effect of the noise on the system is examined. In order to do that, the noise input to the system is opened. Therefore, the third simulation with the step command is done by introducing both the wing rock dynamics and the noise to the system. The block diagram referring to the final simulation of the step command is shown in the Figure 2.14

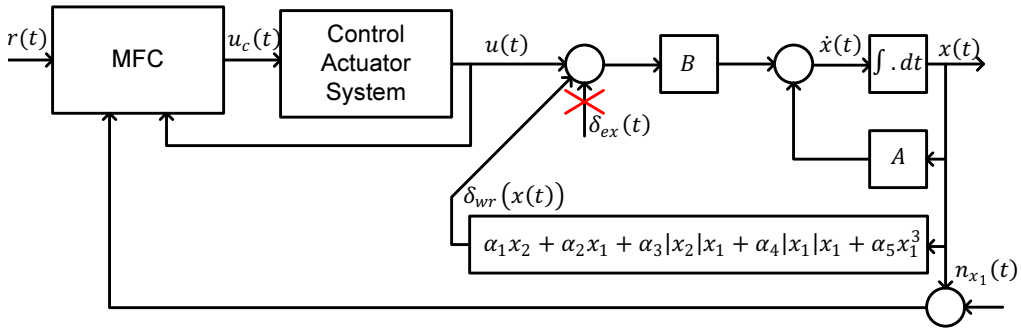

Figure 2.14: MFC block diagram with wing rock dynamics and noise.

The response of the MFC to the step command defined in the Figure 2.9 under the effect of the wing rock dynamics and the random measurement noise with the properties given in 2.4 is shown in the Figure 2.15.

The Figure 2.15 shows the disturbance rejection and noise filtering performance of the MFC at the same time. The controller performs in satisfactory levels for both objectives. The response of the MFC, shown in figure with the green line, follows the reference model roll angle response closely.

The three simulations done for the step command show that the MFC can control the system under the effect of wing rock dynamics and random measurement noise on the roll rate. For an other command set, the MFC is examined in the following subsection 2.4.2.

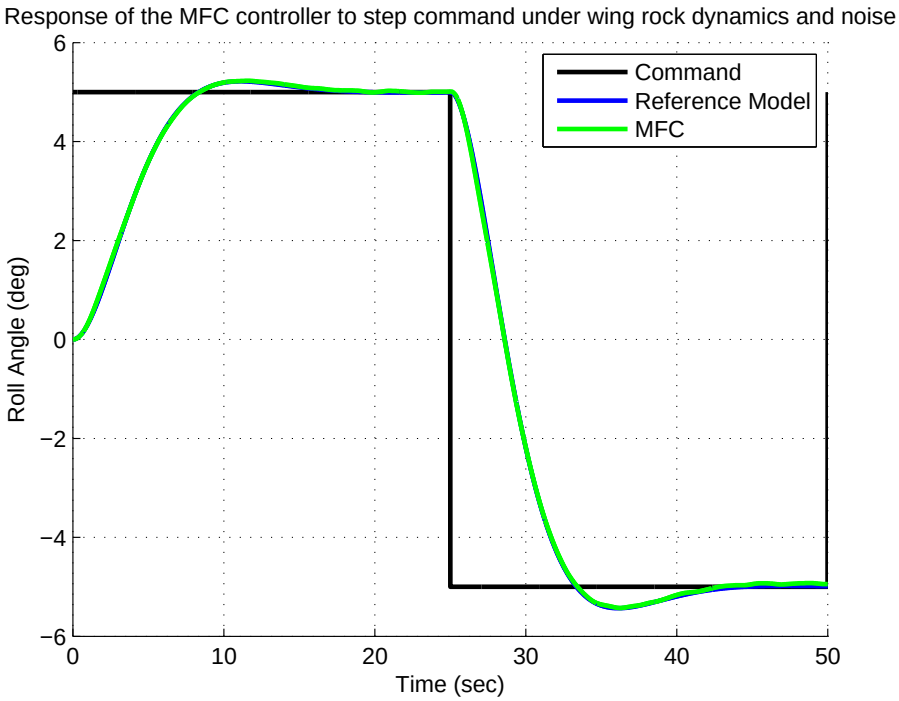

Figure 2.15: MFC response to step command under the effect of wing rock dynamics and noise.

2.4.2 Sinusoidal Command

The reference input to the system controlled with MFC is selected as a sine wave for this subsection. The controller is shown to be robust for the wing rock dynamics and measurement noise while following step command in the previous subsection.

The sine wave command used in the simulation is selected to have a 5 degrees amplitude and $\frac{1}{50}\ Hz$ frequency. The sine wave command is shown in the Figure 2.16.

The comparison for the responses of the MFC under no disturbance and no noise, under only wing rock disturbance, and under both wing rock disturbance and noise is done in the previous subsection. The result of the comparison is that, the controller can deal with both the wing rock disturbance and noise for step command. Therefore, for the sine wave command, only one simulation is done. In this simulation, both the wing rock disturbance and the noise are acting on the system. The block diagram for the simulation is shown in the Figure 2.14.

The response of the MFC for the given sine wave command for the roll angle of the slender delta wing is shown in the Figure 2.17.

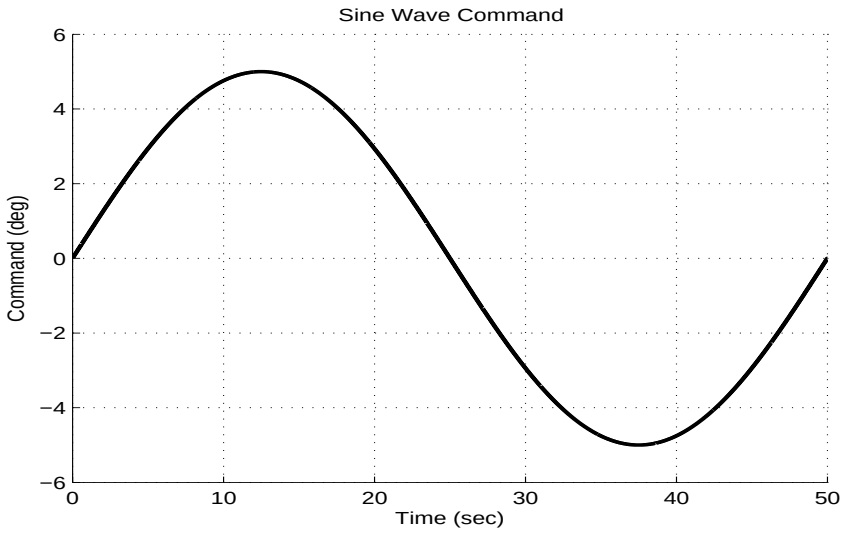

Figure 2.16: Sine wave command input.

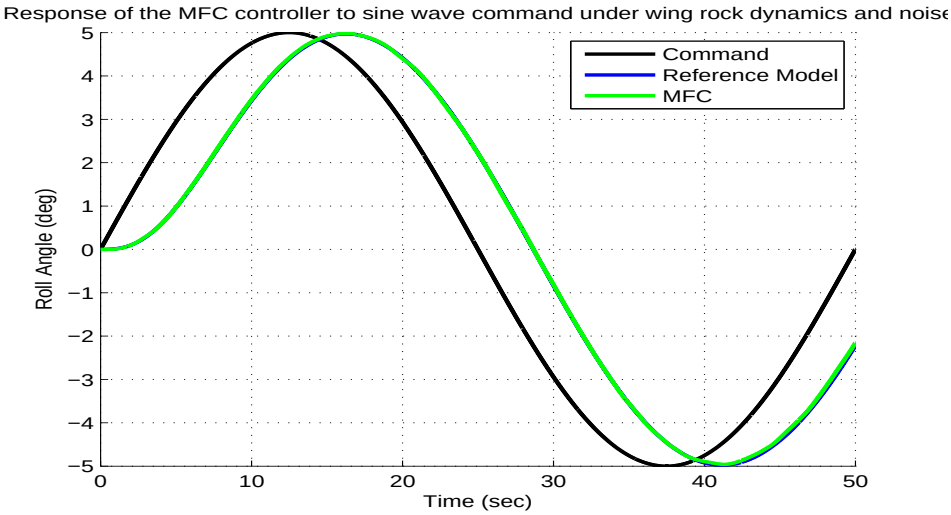

Figure 2.17: MFC response to sine command under the effect of wing rock dynamics and noise.

In the Figure 2.17, the sine wave command is shown with the black line. The reference roll angle calculated by the reference model for he given sine wave command is shown by the blue line, and the roll angle response of the MFC is shown with the green line.

By examining the figure, it can be said that the system controlled with MFC is robust to the defined wing rock dynamics and roll rate measurement noise. This argument states that the design done by using the linear design tools resulted in a satisfactory performance and robustness level. The linear design tools that are used for the design are the optimal gain calculation with the linear quadratic regulation and the frequency

domain analysis tools. These tools are not available for nonlinear controllers, but can be used to state performance of the base controllers such as MFC.

2.5 Challenging Disturbance Case

The robustness and performance of the designed MFC is satisfactory for the given command following needs and disturbances and noise acting on the system. In order to examine controller's robustness to the external disturbances, the difficulty of the acting disturbance is increased.

In addition to the wing rock dynamics $\delta_{wr}(x(t))$, the external disturbance $\delta_{ex}(t)$ which is only a function of time is defined. This disturbance is a random disturbance, and it is only a function of time. This external disturbance is introduced to the system in order to represent the effects due to wind and gust on the system. The random gust can occur for the slender delta wing, and can result to rolling moments on the system. The disturbance input is taken as an equivalent input with the aileron deflection angle, therefore, its dimension is in degrees.

The block diagram representing the system controlled by MFC with disturbance and noise inputs is shown in the Figure 2.8.

For the challenging disturbance case, the selected external disturbance $\delta_{ex}(t)$ is shown in the Figure 2.18.

The random external disturbance shown in the Figure 2.18 has a important property in terms of its frequency content. This external disturbance is created by filtering out high frequency content and the peak frequencies of the data shown in random external disturbance is around $1\ rad/s$. This frequency is where the disturbance rejection magnitude plot of the MFC design makes a peak. Disturbing the designed controller at the frequency around its disturbance rejection transfer function makes a peak results in a challenging disturbances case. This is the main difference of the selected random external disturbance than the acting wing rock dynamics on the system.

The possible gust effects that is possible to occur on the delta wing is simulated with this external disturbance input. The external disturbance has peaks around $+10$

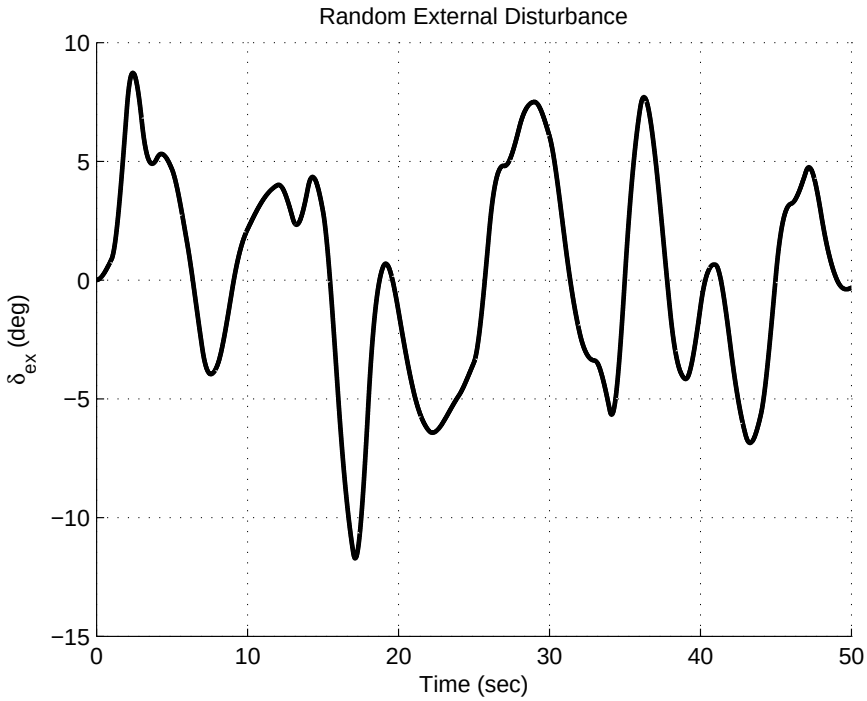

Figure 2.18: Random external disturbance.

degrees and -15 degrees. This numbers mean that, for that amount of gust, the equivalent control input amount is that much degrees. So the controller needs to apply the exact opposite of the external disturbance in order to cancel out the effect of it on the system.

The system controlled with MFC is examined for the wing rock dynamics disturbance and roll rate measurement noise in the previous section 2.4. There are two different command set are used to inspect the robustness and performance of the controller. These command sets are the step command which is formed by repeating step commands in different directions, and sinusoidal command with certain magnitude and frequency. Now, MFC is examined with the same command sets but the external disturbance is included to the system.

The plot of the step command is shown in the Figure 2.9. A simulation is done in order to obtain the the response of the system controlled with MFC under the effect of both the wing rock dynamics $\delta_{wr}\left(x(t)\right)$ and the external disturbance $\delta_{ex}(t)$, and the roll rate measurement noise $n_{x_1}(t)$. The results for the roll angle tracking is shown in the Figure 2.19.

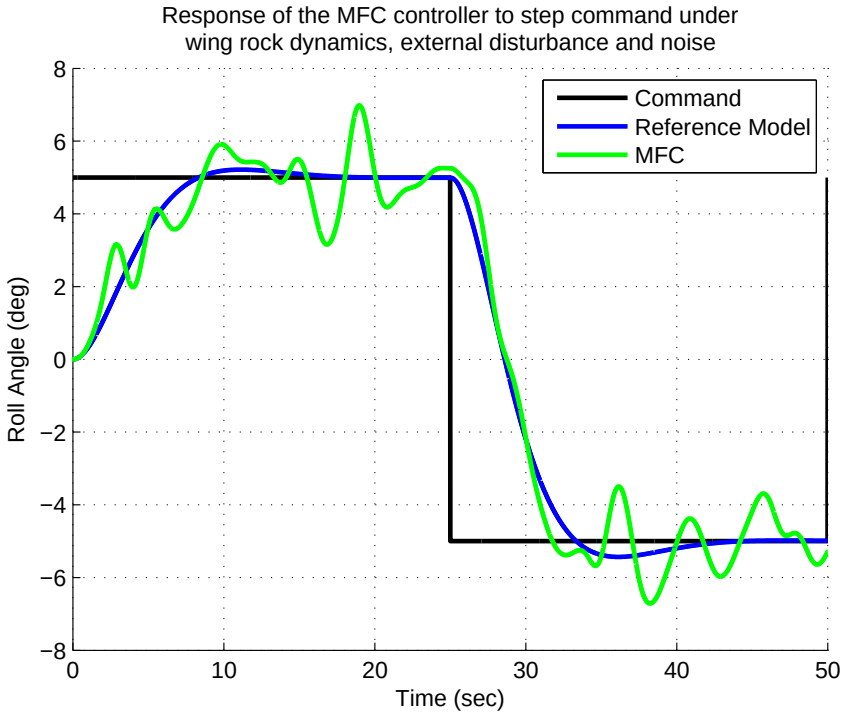

Figure 2.19: MFC response to step command under the effect of wing rock dynamics, external disturbance and noise.

The step command in the Figure 2.19 is shown with the black line. The reference model roll angle response to the applied step command is shown with the blue line. The reference model response is exactly the same with the previous reference model responses, since the reference model is the same. The response of the MFC is shown in the Figure 2.19 with green line. As it can be seen from the figure the response of the controller is degraded when compared with the response shown before. This degradation is occurred due to the introduced external disturbance on the system. This disturbance result in a challenging case. Although the MFC is designed by regarding the disturbance rejection robustness character of the controller to be high enough to eliminate acting disturbances, the response of the controller under given command set and disturbance input seem to have been spoiled. The robustness of the controller is also effecting the response, since the roll angle is succeed to follow the reference roll angle. However, the following performance is not satisfactory.

The wing rock dynamics are nonlinear in terms of the states of the system. In addition, the introduced external disturbance is random in time so the effect of it may change according to the states of the system. Therefore, the command set is changed similar

to the previous section.

The plot of the sine wave command is shown in the Figure 2.16. The simulation is repeated with the exact same external disturbance $\delta_{ex}(t)$ input to the system. The wing rock dynamics and measurement noise are also introduced in this simulations. Only the step command for the roll angle is changed to sine wave command. The result of the simulation is shown in the Figure 2.20.

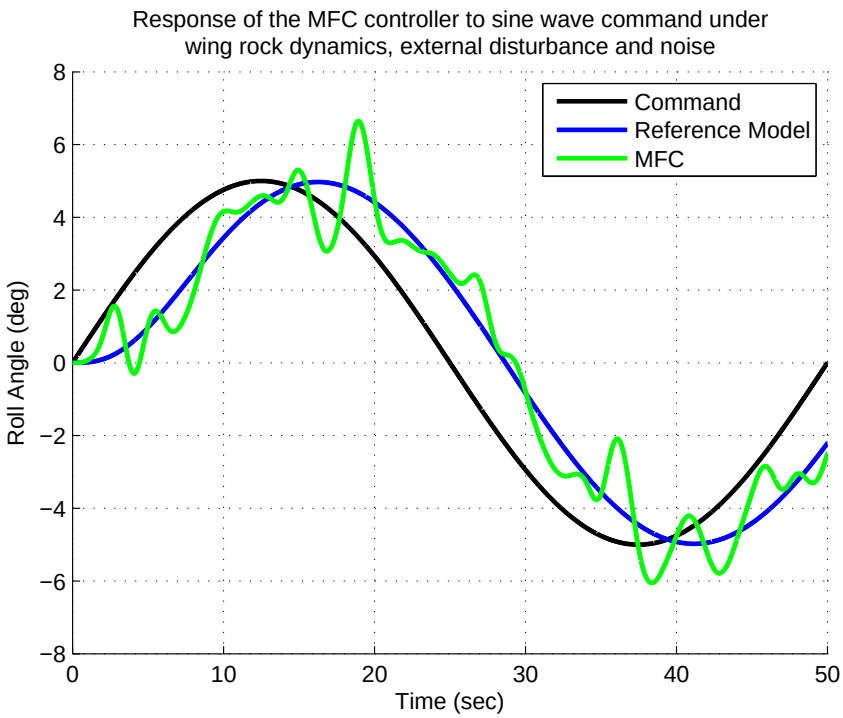

Figure 2.20: MFC response to sine command under the effect of wing rock dynamics, external disturbance and noise.

The commanded sine wave input for the roll angle is shown with the black line in the Figure 2.20. The reference model roll angle response for the commanded sine wave is shown with the blue line. The lag between the commanded sine wave and the reference roll angle is introduced due to the filtering effect of the reference model used. This lag is a result of the designed controller. The response of the system controlled with the MFC is shown with the green line. The roll angle response of the system is again diminished under the effect of the applied external disturbance when compared to the previous simulation done with the sinusoidal command. The effect of the external disturbance on the roll angle response can followed from the Figure 2.20.

First of all, both of the figures Figure 2.19 and Figure 2.20 show that the system controlled with MFC keeps its stability under the given wing rock dynamics, external disturbance input and roll rate measurement noise input. Keeping system stable is not enough in most cases of controllers, so the problem leads to the performance degradation due to the disturbance acting on the system. Next conclusion for the simulation results can be taken as the controller succeed to follow the reference model but with unwanted disruptions in the response. These unwanted disruptions are occurred due to the external disturbance acting on the system.

The simulations with challenging disturbance case lead the designer to a search of finding better controllers for this problem. The possible solution for the problem is searched in the adaptive control methods in the following chapters.

CHAPTER 3

MODEL REFERENCE ADAPTIVE CONTROL

Model reference adaptive control (MRAC) method is one of the most widely used adaptive control method in the literature. Various examples of the MRAC method can be found in [60, 43, 5, 7, 44, 22, 37, 46, 39, 40] and many others.

Similar to the model following control (MFC), the MRAC method uses a reference model to represent the desired system response. An adaptive element is used to adjust the controller input to the system for adapting the changes in the system and unexpected disturbances.

For the basic MRAC, the uncertainty parametrization is done by using known functions of system variables. Using known functions of system variables is equal to knowing the structure of disturbance, but trying to adapt the weightings for the structure. Example studies where the uncertainty parametrization is done by using known functions of system variables can be found in [9, 10, 31, 39, 40, 64, 61, 46, 65].

This chapter is formed by two sections. In the first section, the basic MRAC is represented. In the second section, the simulation is done for the challenging case defined in 2.5 by using the MRAC method. The performance of the controller is discussed.

3.1 Representation of MRAC

The mathematical model representing the MRAC is given on a general system model. Consider a general system model similar to the one given in 2.1 as

$$\dot{x}(t) = Ax(t) + B\left[u(t) + \Delta(t)\right]. \tag{3.1}$$

The state vector is defined by $x(t) \in \mathbb{R}^n$ and the control input is defined by $u(t) \in \mathbb{R}$. For the proceeding argument the general system is assumed to have single input so the control input is $u(t) \in \mathbb{R}$. The disturbance on the system is $\Delta(t) \in \mathbb{R}$. The disturbance is assumed to have the form

$$\Delta(t) = W\beta\left(x(t)\right). \tag{3.2}$$

In (3.2) $\beta\left(x(t)\right)$ represents the uncertainty parametrization for the disturbance estimation. This parametrization is done as functions of the states of the system. The constant ideal weights W is representing the weightings of the corresponding parametrization.

The control input $u(t)$ to the system is calculated by using both the nominal controller and the adaptive controller as

$$u(t) = u_n(t) - u_{ad}(t) \tag{3.3}$$

with dimensions $u_n(t) \in \mathbb{R}$ for nominal control input and $u_{ad}(t) \in \mathbb{R}$ for adaptive control input.

The nominal input $u_n(t)$ is calculated by a full-state feedback. This full-state feedback controller is

$$u_n(t) = -K_r x(t) + K_r H r(t). \tag{3.4}$$

Here the controller gain is $K_r \in \mathbb{R}^{1\times n}$. The reference input to the system is assumed to have dimension of $r(t) \in \mathbb{R}$. The matrix for the reference input is $H \in \mathbb{R}^{n\times 1}$.

The control gain K_r is calculated in such a way that the closed loop system equation for the system controlled with the nominal controller results in the reference model. This means the closed-loop response of the system controlled with the nominal controller with out any disturbance on the system is equal to the desired response.

Hence, the reference model used for the MRAC has the system equation as

$$\begin{aligned} \dot{x}_r(t) &= \left(A - BK_r\right)x_r(t) + BK_r H r(t) \\ \dot{x}_r(t) &= A_r x_r(t) + B_r r(t). \end{aligned} \tag{3.5}$$

The reference model state has the same dimension with the system state as $x_r(t) \in \mathbb{R}^{n\times 1}$. The reference model matrices as can be seen from the reference model equation

are $A_r = A - BK_r \in \mathbb{R}^{n\times n}$ as reference model system matrix and $B_r = BK_rH \in \mathbb{R}^{n\times 1}$ as reference model input matrix.

The aim of the adaptive input is to cancel out the disturbance on the system. Therefore, the adaptive controller input has the same form of the uncertainty parametrization done for the disturbance. The uncertainty parametrization is formed by two multipliers where one of the is a vector formed by the known functions of the system states and the other is weightings regarding each component of the parametrization vector. It is assumed that there are ideal weights for the uncertainty but they are not known by the controller so estimates of these weights are used in the adaptive control input. The adaptive control input is calculated as

$$u_{ad}(t) = \hat{W}(t)\beta\left(x(t)\right) \tag{3.6}$$

The estimated weights $\hat{W}(t)$ have the same dimension with the ideal weights and they are updated in every time step by the adaptive controller.

The weight update law for the MRAC is

$$\dot{\hat{W}}(t) = \Gamma\beta(t)e(t)^T PB. \tag{3.7}$$

In (3.7), the learning rate of the weight update is represented with Γ. The learning rate is a design selection. As the value of the learning rate is increased, the weight is sensitivity of the weight update law to the error between the system states and reference model states increases. Therefore, the adaptation mechanism tries to update weight with high derivatives. This results a faster response on estimating the disturbance on the system. Estimating the disturbance by updating the weighting faster results in a higher learning rate. So, the design selection multiplier Γ of the weight update law is called as the learning rate of the adaptation.

The error shown in (3.7) is equal to the error between the system states and the reference model states. The equation for calculation of the error is

$$e(t) = x(t) - x_r(t) \tag{3.8}$$

where $e(t) \in \mathbb{R}^{n\times 1}$. This element in the update law is used to drive the adaptation mechanism. In case the error between the system states and reference model reaches

to zero, the weightings corresponding the uncertainty parametrization are succeed to be equal to the ideal weights. Therefore, adaptation stops for zero error case. On the other hand, as the error increases, the effect of it on the weight update law increases. This results a higher derivative for weight update. The error drives the adaptation mechanism this way.

The constant matrix P is calculated from the Lyapunov equation which is

$$A_r^T P + P A_r + R = 0. \tag{3.9}$$

The reference model system matrix A_r is used in the Lyapunov equation shown in (3.9). The matrix R is a positive definite design selection matrix. The designer can select any matrix which is positive definite to manipulate the adaptation mechanism of the MRAC.

The Lyapunov stability analysis is omitted in this discussion. The details of the stability proof of the basic MRAC with uncertainty parametrization using known functions of the system states can be found in many numbers of references. A simple explanation for the proof can be found in [62].

The block diagram representing the MRAC is shown in the Figure 3.1

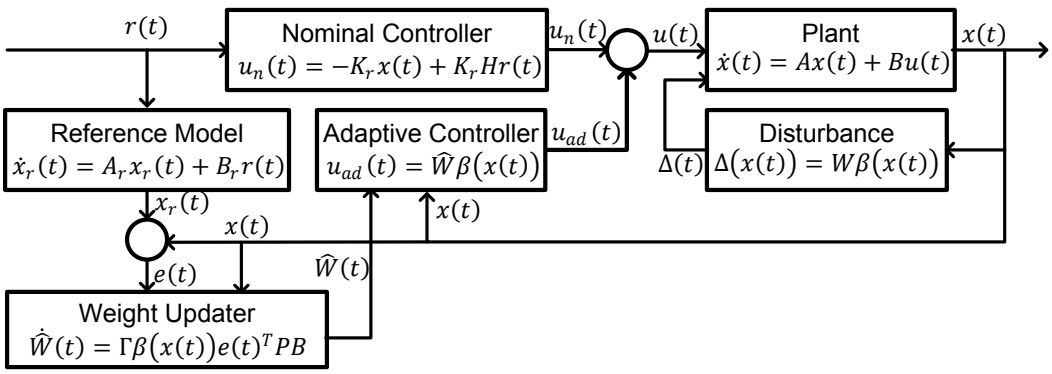

Figure 3.1: MRAC block diagram.

As it can be seen from the figure the weight update law is driven by the error between the system states and the reference model states. The adaptive control input is calculated by the updated weight and subtracted from the nominal controller gain in order to cancel out the uncertainty effect introduced by the disturbance. The uncertainty parametrization $\beta(x(t))$ is assumed to be known and is formed by functions of the system states. Therefore, both the weight update law and adaptive controller use

system states as feedback.

The general overview of the model reference adaptive control method is given in this section. The performance of it for the defined problem will be examined in the following section 3.2

3.2 Simulation for the Challenging Case with MRAC

In this section, the performance of the MRAC method under the challenging case defined previously is inspected. The roll angle control of the slender delta wing system is done by using the MRAC method. The challenging control problem includes the wing rock dynamics given in (2.48). The wing rock disturbance $\delta_{wr}(t)$ is calculated by multiplying the function of system states with ideal weights. This disturbance on the system is ideal for using the MRAC method. This is because of the fact that the MRAC method also uses parametrization of the disturbance by using known functions of the system states.

The wing rock dynamics defined for the delta wing can be rewritten as

$$\begin{aligned}\delta_{wr}(t) &= W\beta\left(x(t)\right) \\ &= \alpha_1 x_2 + \alpha_2 x_1 + \alpha_3 |x_2| x_1 + \alpha_4 |x_1| x_1 + \alpha_5 x_1^3.\end{aligned} \tag{3.10}$$

The system state function vector $\beta\left(x(t)\right)$ in (3.10) is

$$\beta\left(x(t)\right) = \begin{bmatrix} x_2 \\ x_1 \\ |x_2| x_1 \\ |x_1| x_1 \\ x_1^3 \end{bmatrix}. \tag{3.11}$$

The ideal weight vector whose elements correspond the elements in the system state function vector is

$$W = \begin{bmatrix} \alpha_1 & \alpha_2 & \alpha_3 & \alpha_4 & \alpha_5 \end{bmatrix}. \tag{3.12}$$

The numerical value of the ideal weights as mentioned in 2 which is taken from [66]

is

$$\begin{aligned} W &= \begin{bmatrix} \alpha_1 & \alpha_2 & \alpha_3 & \alpha_4 & \alpha_5 \end{bmatrix} \\ &= \begin{bmatrix} 0.1414 & 0.5504 & -0.0624 & 0.0095 & 0.0215 \end{bmatrix} \end{aligned} \tag{3.13}$$

The system equation can be rewritten with the new expression for the wing rock dynamics as

$$\dot{x}(t) = Ax(t) + B\left(u(t) + W\beta\left(x(t)\right) + \delta_{ex}(t)\right). \tag{3.14}$$

The system matrix A and the input matrix B representing the rolling dynamics of a slender delta wing are

$$A = \begin{bmatrix} 0 & 0 \\ 1 & 0 \end{bmatrix} \quad B = \begin{bmatrix} 1 \\ 0 \end{bmatrix}. \tag{3.15}$$

The reference model representing the desired response is calculated by using the pole placement method as mentioned in 2. The desired natural frequency and damping ratio for the reference model are selected as $\omega_n = 0.4\, rad/s$ and $\zeta_n = 0.707$. The reference model and the nominal controller gains K_r are calculated by using the Ackermann's formula. The Ackermann's formula is shown in (2.12). The calculated controller gains are

$$K_r = \begin{bmatrix} 0.57 & 0.16 \end{bmatrix} \tag{3.16}$$

The reference model state space equation is

$$\begin{aligned} \dot{x}_r(t) &= \left(\begin{bmatrix} 0 & 0 \\ 1 & 0 \end{bmatrix} - \begin{bmatrix} 1 \\ 0 \end{bmatrix} \begin{bmatrix} 0.57 & 0.16 \end{bmatrix} \right) x_r(t) + \begin{bmatrix} 1 \\ 0 \end{bmatrix} \begin{bmatrix} 0.57 & 0.16 \end{bmatrix} \begin{bmatrix} 0 \\ 1 \end{bmatrix} r(t) \\ \dot{x}_r(t) &= \begin{bmatrix} -0.57 & -0.16 \\ 1 & 0 \end{bmatrix} x_r(t) + \begin{bmatrix} 0.16 \\ 0 \end{bmatrix} r(t) \end{aligned}. \tag{3.17}$$

So the reference model in compact form is

$$\dot{x}_r(t) = A_r x_r(t) + B_r r(t). \tag{3.18}$$

The nominal controller used in the MRAC is

$$u_n(t) = -K_r x(t) + K_r H r(t) \tag{3.19}$$

where the selection matrix is

$$H = \begin{bmatrix} 0 \\ 1 \end{bmatrix} \tag{3.20}$$

The numerical representation of the nominal controller is

$$u_n(t) = -\begin{bmatrix} 0.57 & 0.16 \end{bmatrix} + 0.26\, r(t). \tag{3.21}$$

The adaptive part of the MRAC is calculated with

$$u_{ad}(t) = \hat{W}(t)\beta\left(x(t)\right). \tag{3.22}$$

The parametrization vector $\beta\left(x(t)\right)$ is assumed to be known. The dimension of the vector is $\beta\left(x(t)\right) \in \mathbb{R}^{5\times 1}$. The dimension of the weightings of the parametrization vector is $W \in \mathbb{R}^{1\times 5}$. The estimated weights need to be calculated by the weight update law. The weight update law is

$$\dot{\hat{W}}(t) = \Gamma\beta(t)e(t)^T PB. \tag{3.23}$$

The learning rate Γ in the weight update law has the dimension $\Gamma \in \mathbb{R}^{5\times 5}$ and is selected as a design selection. For the MRAC design in this study, the learning rate is selected as

$$\Gamma = \begin{bmatrix} 10 & 0 & 0 & 0 & 0 \\ 0 & 10 & 0 & 0 & 0 \\ 0 & 0 & 10 & 0 & 0 \\ 0 & 0 & 0 & 10 & 0 \\ 0 & 0 & 0 & 0 & 10 \end{bmatrix} \tag{3.24}$$

This selection is done by trial and errors. The trade off between increasing and decreasing the learning rate is lying between the instability and insensitively. Increasing the learning rate more than the selected value, the robustness of the system decreases. For further increase in the learning rate results in unstable system under defined disturbances. Lowering the learning rate results slower response from the adaptive element so the adaptation becomes insensitive to the disturbances. As a trade off study, the learning rate shown in (3.24) is selected.

The matrix P in (3.23) is calculated by the Lyapunov equation shown in (3.9). The R matrix used in the Lyapunov equation is also an other design selection. This matrix is selected as

$$R = \begin{bmatrix} 1000 & 0 \\ 0 & 0.01 \end{bmatrix}. \tag{3.25}$$

The selection of the R matrix effects the sensitivity of the adaptation on the error. Each diagonal element in the R matrix corresponds to the elements in the error vector. The error vector is defined as the difference between the system states and the reference model states. In the example of the slender delta wing, system states are the roll rate and the roll angle. Therefore, by changing the diagonal elements of the R matrix, the sensitivity of the adaptive law to the each of the system states can be manipulated. By trying several values for the R matrix and examining the simulations the values shown in (3.25) are selected.

For examining the challenging case, two sets of inputs used. These inputs are the stair step command shown in the Figure 2.9 and the sine wave command shown in the Figure 2.16.

The simulations are done including wing rock dynamics $\delta_{wr}\left(x(t)\right)$ defined in (3.10), external random disturbance $\delta_{ex}(t)$ shown in the Figure 2.18, and the roll rate measurement noise defined in 2.4.

The block diagram of the system controlled by using the MRAC is shown in the Figure 3.1. The control actuator system is not shown in this figure. It is also not included to the design of the controller. However, the control actuator system, with the properties defined in 2.1, is used in the simulations.

The measurement of the states is assumed to be fast enough to neglect, and the measurement dynamics are neglected.

The response of the MRAC under the given disturbances and noise for the step command is shown in the Figure 3.2

As can be seen from the Figure 3.2, the model reference adaptive control can not give a satisfactory command following performance under defined disturbances. This is a result of the fact that the controller assumes a wrong structure for the uncertainty. This can be shown simply by removing the external disturbance and repeating the same simulation with only wing rock dynamics acting. By making this change in the simulations is giving the MRAC full control of the disturbance on the system.

Knowing the structure disturbance on the system is not a wide covering case for many

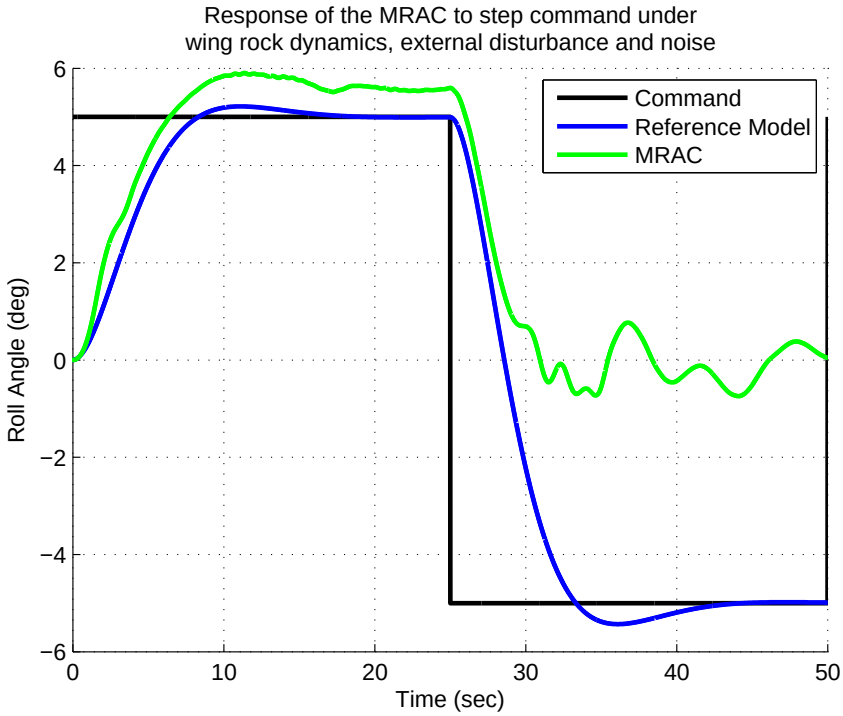

Figure 3.2: MRAC response to step command under the effect of wing rock dynamics, external disturbance and noise.

of the applications especially those occurring on open air. The delta wing isopen to the any kind of possible disturbances. For now on, just to see if the designed controller is capable of eliminating the wing rock dynamics by estimating the weightings of the nonlinear functions of system states, a simulation with only wing rock dynamics and measurement noise acting on the system is done. The command is kept as step command. The response of the system to the step command is shown in the Figure 3.3

As can be seen from the Figure 3.3, the command tracking performance of the MRAC increases fairly compared to the case where the external disturbance is acting.

The simulations with step command shows that, the MRAC method can not cancel out the unwanted effect of the external disturbance acting on the system. The controller has nonlinear component such as weight update law and adaptive control input calculation. Due to this non-linearity, an other simulation with a different command set is done. The next command set is the sine wave command.

The sine wave command is defined in 2.4.2, and plot of it is shown in the Figure 2.16. The simulation of the system with wing rock dynamics, external disturbance and

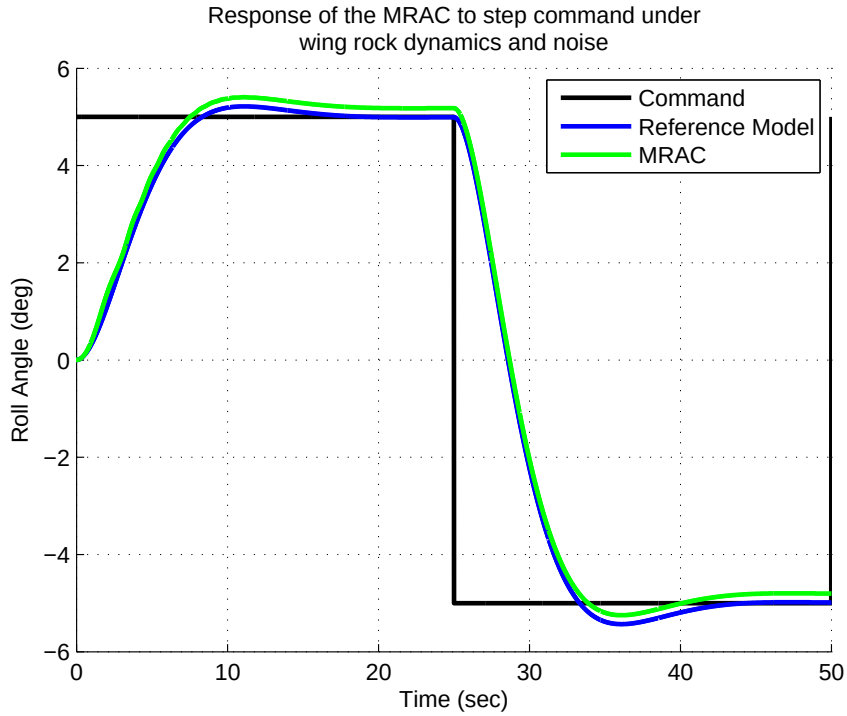

Figure 3.3: MRAC response to step command under the effect of wing rock dynamics and noise.

measurement noise is done. The response of the MRAC to the sine wave command is shown in the Figure 3.4.

As it can be seen from the Figure 3.4, the controller designed using the MRAC method is failed to follow the given sine command. This is an expected result.

The MRAC is designed to overcome the uncertainties which have the predefined structure. The external disturbances that are not included inside the uncertainty parametrization of the MRAC are cause impairment on the system response to a given command.

This situation is occurring due to the selection of the uncertainty parametrization. Assuming the disturbance acting on the system is a combined function of the system states and in addition assuming this function is known can result a response shown in Figure 3.4.

The design of the MRAC controller is tried to be done in such a way that it can endure the given disturbances. However, limiting the structure of the disturbance may act on the system is not an helping choice.

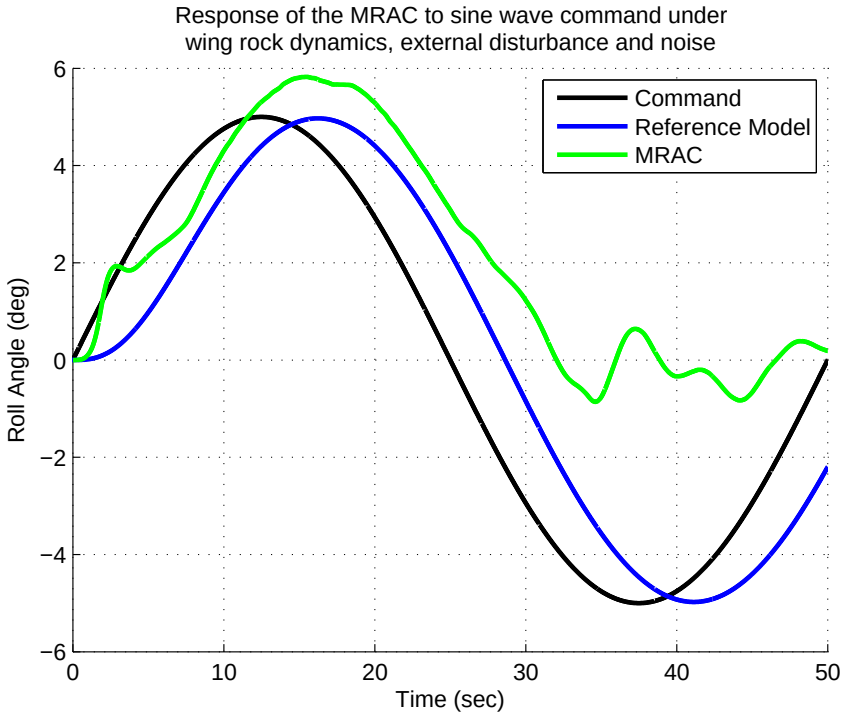

Figure 3.4: MRAC response to sine command under the effect of wing rock dynamics, external disturbance and noise.

The robustness and performance of the MRAC can be improved by using several modification terms that are introduce in the literature. However, in the scope of this study, simulations using these modifications are omitted.

In stead of applying modification terms on the MRAC, a new uncertainty parametrization method is proposed. This method is explained in detail in the following chapter 4

In the chapter 3, the representation of the well known MRAC with uncertainty parametrization using known functions of system states is done. Then, simulations for the challenging case raised in 2.5 is conducted. Finally, the non-satisfactory results of the simulations for the MRAC are demonstrated.

CHAPTER 4

FOURIER SERIES BASED MRAC

Any function that is periodic can be represented with a Fourier series. Representing a function with a Fourier series means forming that function by using simple periodic functions. These periodic functions are sine and cosine functions. Summation of these simple sine and cosine functions with a certain weighting results in any periodic function.

In this chapter, a novel method for uncertainty parametrization is proposed. This approach depends the powerful representation competence of the Fourier series.

The disturbance acting on the system is assumed to have a periodic nature. Moreover, an attempt to satisfy this assumption is done by manipulating the period of the periodic function. The periodic disturbance is estimated using the powerful Fourier series. This estimation mechanism is used as basis to the model reference adaptive control. In other words, the uncertainty on the system is parametrized by using Fourier series. The sine and cosine functions forming the Fourier series are kept as variable vector in the adaptive element and the weightings are estimated to match the disturbance and cancel its effect on the system.

In this chapter, first the stability proof of the proposed method is shown. After that, performance of the novel method proposed is examined for the challenging case by using simulation. Next, the effect of unmodeled dynamics is inspected. Then, the effect of the sampling time used to calculate the controller inputs is examined. Then, a mathematical comparison for disturbance rejection character of the controller is done. Finally, the controller is examined with different and challenging random dis-

turbances.

4.1 Stability Proof for Fourier Series Based MRAC

Considering the general nonlinear dynamical system given by

$$\dot{x}(t) = Ax(t) + B[u(t) + \Delta(t)], \quad x(0) = x_0 \quad t \in \bar{\mathbb{R}}_+ \tag{4.1}$$

where $x(t) \in \mathbb{R}^n$ is the state vector, $u(t) \in \mathbb{R}^m$ is the control input vector, $\Delta(t) \in \mathbb{R}^m$ is uncertainty, $A \in \mathbb{R}^{n\times n}$ is a known system matrix, and $B \in \mathbb{R}^{n\times m}$ is a known control input matrix.

Assumption 4.1.1 *The uncertainty $\Delta(t)$ is periodic function with a period of T, so it can be represented by Fourier series.*

A function $f(t)$ is called periodic if it repeats itself in a period. The repetitive character of a function $f(t)$ can be shown by the equation given in (4.2).

$$f(t) = f(t + T) \tag{4.2}$$

A known example of periodic function is shown in the Figure 4.1.

This assumption is not a restrictive assumption since any function with a finite operation time can be taken as a periodic function. For example, take the function $f(t) = t$ which is clearly not a periodic function, and state that this function has a finite operation time so that $f(t) = t \quad \forall t \in [0, t_f]$. If so, the function $f(t)$ can be perfectly represented with a Fourier series expansion given long enough period and series length. The equation for the Fourier series expansion is shown in

$$f(t) \cong F(t) = a_0 + \sum_{k=1}^{N} a_k cos\left(k\frac{2\pi}{T}t\right) + b_k sin\left(k\frac{2\pi}{T}t\right). \tag{4.3}$$

The coefficients a_0, a_k, and b_k are called as Fourier series coefficients. The index k shows the coefficient number, and N shows the series length. The Fourier series coefficients a_0, a_k, and b_k can be calculated by the equations shown in (4.4), (4.5),

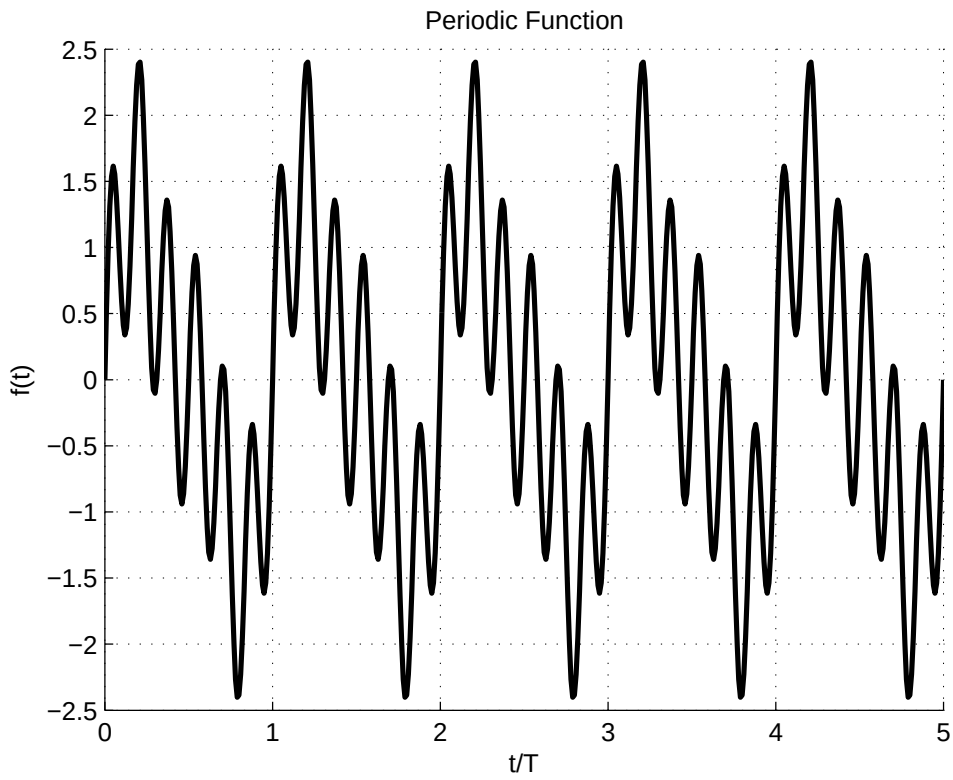

Figure 4.1: Periodic function.

and (4.6), respectively.

$$a_0 = \frac{1}{T}\int_{-T/2}^{T/2} f(t)dt \tag{4.4}$$

$$a_k = \frac{2}{T}\int_{-T/2}^{T/2} f(t)cos(k\frac{2\pi}{T}t)dt \tag{4.5}$$

$$b_k = \frac{2}{T}\int_{-T/2}^{T/2} f(t)sin(k\frac{2\pi}{T}t)dt \tag{4.6}$$

These coefficients are scalar constant for given function $f(t)$.

The selection of the period of the Fourier series expansion is critical since it affects the representation of the function $f(t)$ with the expansion equation (4.3). The period T should be at least 3 times longer than the operation time. This relation can be seen in the Figure 4.2.

As seen in the Figure 4.2, selecting the period of the Fourier series expansion 3 times longer than the operation time gives satisfactory representation.

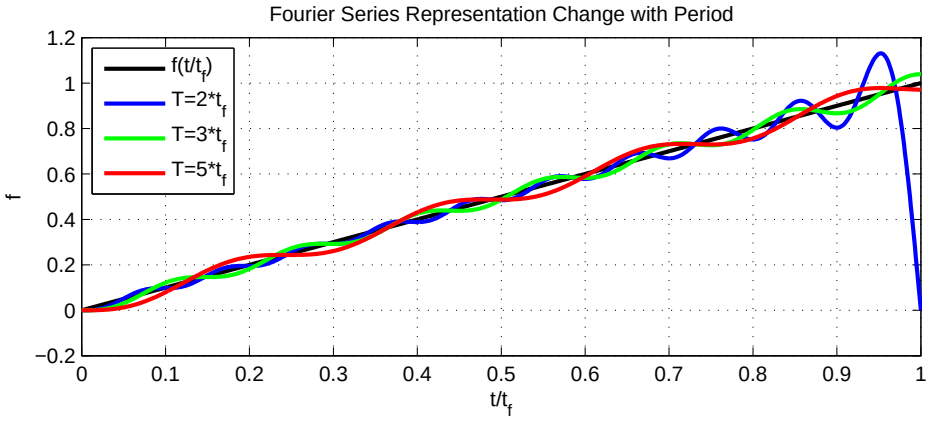

Figure 4.2: Fourier series representation of $f(t)$.

The length of the Fourier series is also an effective component of the expansion. The effect of the series length is shown in the Figure 4.3.

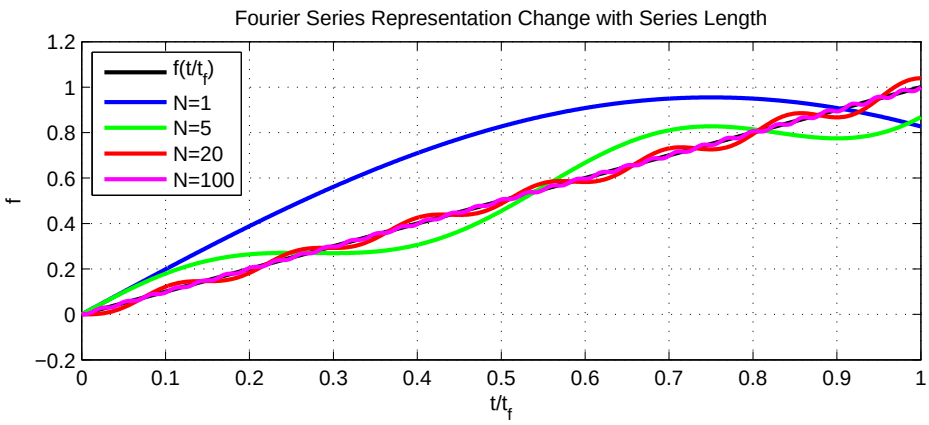

Figure 4.3: The effect of the series length for Fourier series representation of $f(t)$.

The error of the Fourier series expansion is

$$\varepsilon(t) = f(t) - F(t). \tag{4.7}$$

The error $\varepsilon(t)$ decreases as the series length N increases as can be seen in the Figure 4.3. On the other hand, as the series length increases, amount of the coefficients used for the expansion inevitably increases.

The uncertainty $\Delta(t)$ shown in general nonlinear dynamical system given in (4.1) can be represented with Assumption 4.1.1 as follows;

$$\Delta(t) = \left[a_0 + \sum_{k=1}^{N} a_k cos(k\frac{2\pi}{T}t) + b_k sin(k\frac{2\pi}{T}t)\right] + \varepsilon(t) \tag{4.8}$$

The error made by the Fourier series expansion has the same dimensions with the uncertainty, which is $\varepsilon \in \mathbb{R}^m$, and the Fourier series coefficients have the following dimensions; $a_0 \in \mathbb{R}^{m\times 1}$, $a_k \in \mathbb{R}^{m\times 1}$, $b_k \in \mathbb{R}^{m\times 1}$ for $k \in [1, N]$. The summation operation used in (4.8) can be replaced with vector multiplication. The Fourier series coefficients form the first vector of constants and the harmonic functions of times form the second variable vector. This representation of the uncertainty is shown in (4.9).

$$\Delta(t) = \begin{bmatrix} a_0 & a_1 & a_2 & ... & a_N & b_1 & b_2 & ... & b_N \end{bmatrix} \begin{bmatrix} 1 \\ cos\left(1\frac{2\pi}{T}t\right) \\ cos\left(2\frac{2\pi}{T}t\right) \\ ... \\ cos\left(N\frac{2\pi}{T}t\right) \\ sin\left(1\frac{2\pi}{T}t\right) \\ sin\left(2\frac{2\pi}{T}t\right) \\ ... \\ sin\left(N\frac{2\pi}{T}t\right) \end{bmatrix} + \varepsilon(t) \quad (4.9)$$

Equation (4.9) can be represented in compact form by

$$\Delta(t) = W^T\beta(t) + \varepsilon(t) \quad (4.10)$$

where $W \in \mathbb{R}^{m\times p}$ is the Fourier series weights of the uncertainty, and$\beta(t) \in \mathbb{R}^{p\times 1}$ is the cosine and sine functions vector with increasing frequencies. The dimension p is related with the series length N as $p = 2N + 1$.

The desired response of the system is represented with the following reference model,

$$\dot{x}_m(t) = A_m x_m(t) + B_m r(t), \quad x_m(0) = x(0) = x_0 \quad t \in \bar{\mathbb{R}}_+ \quad (4.11)$$

where $x_m(t) \in \mathbb{R}^{n\times 1}$ is the reference model state vector, $r(t) \in \mathbb{R}^{r\times 1}$ is the reference input to the system, $A_m \in \mathbb{R}^{n\times n}$ is the reference system matrix, and $B_m \in \mathbb{R}^{n\times n}$ is the reference input matrix. The reference system matrix A_m is Hurwitz.

Reference model matrices are obtained from system model matrices with the linear relation shown in (4.12).

$$A_m = A - BK_1 \qquad B_m = BK_2 \tag{4.12}$$

The gain $K_1 \in \mathbb{R}^{m\times n}$ is the state feedback gain of the nominal controller and the gain $K_2 \in \mathbb{R}^{m\times r}$ is the reference input gain. The gain K_1 is selected in such a way that it guaranties that the reference system model matrix A_m is Hurwitz.

The augmenting control law for the adaptive controller is shown in (4.13).

$$u(t) = u_n(t) - u_{ad}(t) \tag{4.13}$$

The control input $u_n \in \mathbb{R}^{m\times 1}$ stands for the nominal and $u_{ad} \in \mathbb{R}^{m\times 1}$ stands for the adaptive controller inputs.

Nominal controller input u_n uses both the feedback gain K_1 and reference input gain K_2. The equation of the nominal feedback control law is shown in (4.14).

$$u_n(t) = -K_1 x(t) + K_2 r(t) \tag{4.14}$$

The adaptive controller input has the same form with the uncertainty $\Delta(t)$ on the system. The equation for $u_{ad}(t)$ is;

$$u_{ad}(t) = \hat{W}(t)^T \beta(t). \tag{4.15}$$

The estimated weights $\hat{W}(t) \in \mathbb{R}^{m\times p}$ used in the adaptive controller input are the estimations of the adaptation for the Fourier series coefficients.

The error between the system states and the reference model states is defined as the error of the system with

$$e(t) = x(t) - x_m(t). \tag{4.16}$$

where $e(t) \in \mathbb{R}^{n\times 1}$ is the error state vector.

The dynamics of the error state $e(t)$ is examined by subtracting the dynamic equation of the reference model (4.11) from the system dynamics (4.1). The error dynamics is

$$\dot{e}(t) = \dot{x}(t) - \dot{x}_m(t) = Ax(t) + B[u_n(t) - u_{ad}(t) + \Delta(t)] - A_m x_m(t) - B_m r(t). \tag{4.17}$$

The uncertainty $\Delta(t)$ is replaced by (4.10) and the result is

$$\dot{e}(t) = Ax(t) + B[u_n(t) - u_{ad}(t) + W^T\beta(t) + \varepsilon(t)] - A_m x_m(t) - B_m r(t). \tag{4.18}$$

The equation (4.18) can be reorganized as follows

$$\begin{aligned}\dot{e}(t) &= Ax(t) - BK_1x(t) + BK_2r(t) - Bu_{ad}(t) + BW^T\beta(t) + B\varepsilon(t) \\ &\quad - A_mx_m(t) - B_mr(t),\end{aligned} \tag{4.19}$$

and by replacing corresponding terms in (4.19) by the reference system and input matrix according to the relation shown in (4.12), the error dynamic equation takes the following form

$$\begin{aligned}\dot{e}(t) &= A_mx(t) + B_mr(t) - B\hat{W}(t)^T\beta(t) + BW^T\beta(t) + B\varepsilon(t) \\ &\quad - A_mx_m(t) - B_mr(t).\end{aligned} \tag{4.20}$$

From the definition of the error state the equation can be rewritten as

$$\dot{e}(t) = A_me(t) - B(\hat{W}(t) - W)^T\beta(t) + B\varepsilon(t). \tag{4.21}$$

The error of the weight is defined by the difference between the Fourier series coefficients representing the uncertainty and the estimated weights. The equation for the weight error is $\tilde{W}(t) = \hat{W}(t) - W$. Putting the weight error $\tilde{W}(t)$ in to (4.21) gives

$$\dot{e}(t) = A_me(t) - B\tilde{W}(t)^T\beta(t) + B\varepsilon(t). \tag{4.22}$$

Assumption 4.1.2 *Here it is assumed that for the time being, the Fourier series expansion can represent the uncertainty perfectly and makes no error*

$$\varepsilon(t) = 0. \tag{4.23}$$

This assumption is relaxed below discussions.

4.1.1 Parameric Uncertainty

The stability of the proposed controller is inspected under the parametric uncertainty assumption.

Theorem 4.1.1 *For the Lyapunov function candidate*

$$\mathcal{V}(e(t), \tilde{W}(t)) = \frac{1}{2}e(t)^TPe(t) + \frac{1}{2}tr(\tilde{W}(t)^T\Gamma^{-1}\tilde{W}(t)), \tag{4.24}$$

and for the weight update law

$$\dot{\hat{W}}(t) = \Gamma\beta(t)e(t)^T PB \tag{4.25}$$

with the Lyapunov function properties

$$\mathcal{V}(e(t), W(t)) \geq 0 \quad and \quad \dot{\mathcal{V}}(e(t), W(t)) \leq 0 \tag{4.26}$$

the controller

$$u = u_n - u_{ad} = -K_1 x(t) + K_2 r(t) - \hat{W}^T \beta(t) \tag{4.27}$$

is stable under the Assumption 4.1.2 $(\varepsilon = 0)$.

The proof of this theorem is discussed in several studies and a detailed version of it can be found at Appendix A.

4.1.2 Non-parametric Uncertainty

Assuming the Fourier series expansion to be perfectly representing the uncertainty on the system is a restrictive assumption and needed to be relaxed. Therefore, Assumption 4.1.2 is removed and becomes

$$\varepsilon \neq 0, \tag{4.28}$$

and the weight update law is modified with the following equation

$$\dot{\hat{W}}(t) = \Gamma\left(\beta(t)e(t)^T PB - \sigma\hat{W}(t)\right). \tag{4.29}$$

Theorem 4.1.2 *For the Lyapunov function candidate*

$$\mathcal{V}(e(t), \tilde{W}(t)) = \frac{1}{2}e(t)^T Pe(t) + \frac{1}{2}tr(\tilde{W}(t)^T \Gamma^{-1}\tilde{W}(t)), \tag{4.30}$$

and the weight update law

$$\dot{\hat{W}}(t) = \Gamma\left(\beta(t)e(t)^T PB - \sigma\hat{W}(t)\right). \tag{4.31}$$

if for any value of $e(t)$ *one of the bound conditions*

$$\|e(t)\|_2 \geq \sqrt{\left(\frac{\varepsilon^* \|PB\|_F}{\lambda_{min}(R)}\right)^2 + \frac{\left(\frac{\sigma\|W\|_F}{2\sqrt{\sigma}}\right)^2}{\frac{1}{2}\lambda_{min}(R)}} + \frac{\varepsilon^* \|PB\|_F}{\lambda_{min}(R)} \tag{4.32}$$

or

$$\|\tilde{W}(t)\|_F \geq \sqrt{\frac{\left(\frac{\varepsilon^*\|PB\|_F}{2\sqrt{\frac{1}{2}\lambda_{min}(R)}}\right)^2}{\sigma} + \left(\frac{\|W\|_F}{2}\right)^2} + \frac{\|W\|_F}{2} \tag{4.33}$$

holds the controller

$$u = u_n - u_{ad} = -K_1 x(t) + K_2 r(t) - \hat{W}^T \beta(t) \tag{4.34}$$

is stable.

The proof of this theorem is discussed in several studies and a detailed version of it can be found at Appendix B.

4.2 Simulation for the Challenging Case with Fourier Series Based MRAC

In this section, first the design of the Fourier series based MRAC is discussed. Next, the simulation results compared with the controllers mentioned in the previous chapters are shown.

4.2.1 Fourier Series Based MRAC Design for Sample System

The Fourier series based MRAC design is done for the slender delta wing system model represented in 2.1. The system model equation is

$$\dot{x}(t) = \begin{bmatrix} 0 & 0 \\ 1 & 0 \end{bmatrix} x(t) + \begin{bmatrix} 1 \\ 0 \end{bmatrix} \left(u(t) + \delta_{wr}\left(x(t)\right) + \delta_{ex}(t)\right). \tag{4.35}$$

For the reference model design, the same desired character is selected. The desired natural frequency and damping ratio for the reference model are selected as $\omega_n = 0.4\, rad/s$ and $\zeta_n = 0.707$.

The reference model has the same form shown in (3.5).

The nominal part of the controller is the same with the selected reference model. The gains for the nominal controller is calculated by using the Ackermann's formula. The calculated gains for the system to have the desired characteristics in the closed loop

response are

$$K_r = \begin{bmatrix} 0.57 & 0.16 \end{bmatrix}. \tag{4.36}$$

The nominal controller is in the form

$$u_n(t) = -K_r x(t) + K_r H r(t) \tag{4.37}$$

where $H = \begin{bmatrix} 0 \\ 1 \end{bmatrix}$.

The adaptive control element is formed with the Fourier series. The Fourier series based basis function is collection of the sine and cosine terms with different frequencies. The basis function vector for a series length of N is

$$\beta(t) = \begin{bmatrix} 1 \\ cos\left(1\frac{2\pi}{T}t\right) \\ cos\left(2\frac{2\pi}{T}t\right) \\ \dots \\ cos\left(N\frac{2\pi}{T}t\right) \\ sin\left(1\frac{2\pi}{T}t\right) \\ sin\left(2\frac{2\pi}{T}t\right) \\ \dots \\ sin\left(N\frac{2\pi}{T}t\right) \end{bmatrix}. \tag{4.38}$$

The basis function has the dimension of $2N + 1$. This dimension is found as N terms for cosine functions, N terms for sine functions and 1 term for bias.

For the design of the controller for delta wing system, the series length of the Fourier series is selected as $N = 10$. Therefore, the basis function has the dimension of 21.

Next thing to be selected for the design of the Fourier series based MRAC is the longest period of the periodic functions in the basis function vector. This period selection should be done by taking the operating time of the system into account. The simulations for the roll control of slender delta wing is done for 50 seconds. As it is shown in the Figure 4.2, the period of the Fourier series should be selected at least

3 times longer than the operation time. In order to have guarantied performance, the period T of the Fourier series is selected as $T = 200sec$.

The Fourier series is formed by selecting both the series length N and the period T. Now, the adaptive controller parameters selected.

The learning rate for the weight update law is selected as

$$\Gamma = 2\,10^{-1} I_{21\times 21}. \tag{4.39}$$

The matrix $I_{21\times 21}$ is the identity matrix of dimension 21×21.

The design selection matrix R of the Lyapunov equation is selected as

$$R = \begin{bmatrix} 1000 & 0 \\ 0 & 0.01 \end{bmatrix}. \tag{4.40}$$

The selection of the R matrix is exactly the same with the selection of the R matrix used in the MRAC design done in the previous chapter 3. The adaptive control input is calculated as

$$u_{ad}(t) = \hat{W}(t)\beta(t). \tag{4.41}$$

The weighting vector $\hat{W}(t)$ is the estimation of the ideal weights of the ideal Fourier series. This vector can be shown as

$$\hat{W}(t) = \begin{bmatrix} \hat{a}_0 & \hat{a}_1 & \hat{a}_2 & ... & \hat{a}_{10} & \hat{b}_1 & \hat{b}_2 & ... & \hat{b}_{10} \end{bmatrix}. \tag{4.42}$$

The weight update law is

$$\dot{\hat{W}}(t) = \Gamma\left(\beta(t)e(t)^T PB - \sigma\hat{W}(t)\right). \tag{4.43}$$

where the damping modification term is selected as $\sigma = 100$. The block diagram of the Fourier series based MRAC for the system defined is shown in the Figure 4.4

The robustness and performance of the designed controller are discussed in the following section.

4.2.2 Simulation Results for the Challenging Case

The performance and disturbance rejection character of the designed Fourier series based MRAC is examined using simulations. Similar to the simulations in the previous chapters, the simulation for the system controlled with Fourier series based

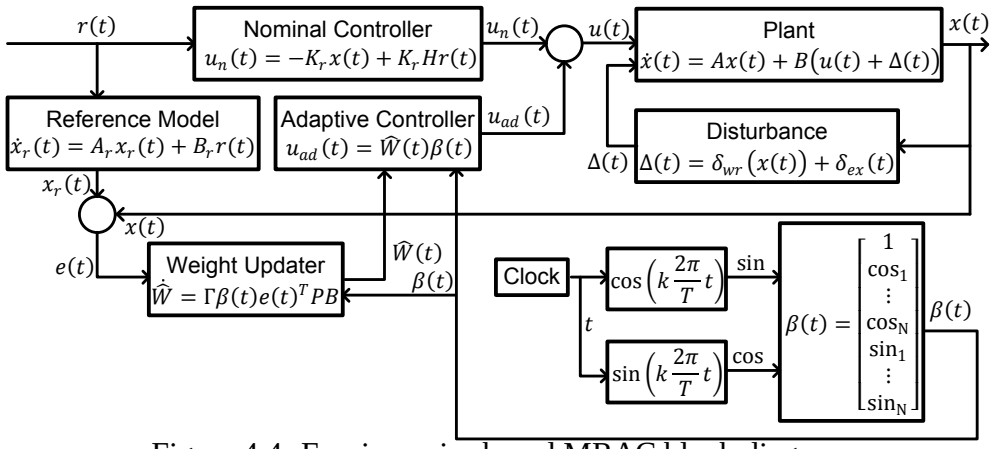

Figure 4.4: Fourier series based MRAC block diagram.

MRAC includes the wing rock dynamics, the external disturbance and the roll rate measurement noise.

The control command is applied to the control actuator system and the control deflection is calculated after passing control actuator system dynamics.

The wing rock dynamics are the same dynamics defined in (2.4). These dynamics are

$$\delta_{wr}(x(t)) = \begin{bmatrix} 0.1414 & 0.5504 & -0.0624 & 0.0095 & 0.0215 \end{bmatrix} \begin{bmatrix} x_2 \\ x_1 \\ |x_2|x_1 \\ |x_1|x_1 \\ x_1^3 \end{bmatrix}. \quad (4.44)$$

The external random disturbance that is modeled for the gust effect may occur on the flight is also included into the system. The plot of the modeled random disturbance is shown in the Figure 2.18. The effect of this disturbance is applied at the control input location of the system and controller is expected to get rid of the unwanted effects introduced by the external disturbance.

The measurement noise acting on the system is the same noise used for the previous simulations. The character of the roll rate measurement noise is given in section 2.4.

Two different sets of commands are applied in the simulations. One is the step command that is shown in the Figure 2.9. The other one is the sine wave command shown in the Figure 2.16.

The command tracking performance of the Fourier series based MRAC under the challenging case disturbance and noise for the step command is shown in the Figure 4.5.

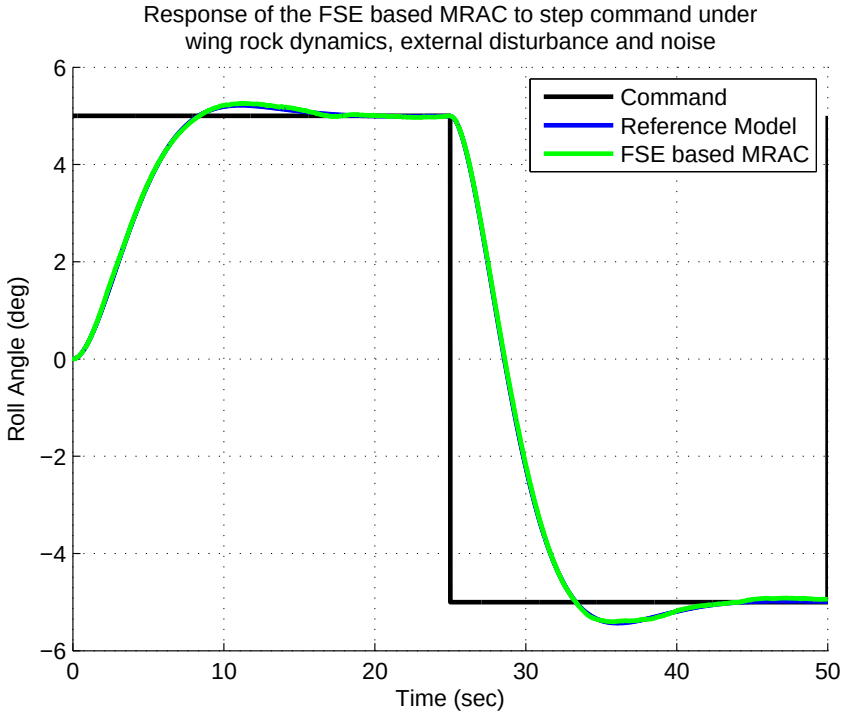

Figure 4.5: Response of the Fourier series based MRAC to step command under the effect of wing rock dynamics, external disturbance and noise.

The command following performance of the Fourier series based MRAC design is much better than the other controllers shown before. The effect of the disturbance acting on the system is almost totally removed from the system.

The comparison of the controllers is done. The MFC, the MRAC and the Fourier series based MRAC controllers' responses to step command under the wing rock dynamics, external disturbance and measurement noise are shown in the Figure 4.6.

As it can be seen from the Figure 4.6, the Fourier series based MRAC follows the reference model roll angle really closely. The other adaptive controller is failed to follow the command satisfactorily. This failure is due to the selection of the uncertainty parametrization. The linear controller augmented with a reference model succeeds to follow the reference model roll angle. However, the effect of the disturbance on the system can be seen from the response of the MFC. Although, the MFC accomplished to follow the reference model, the disturbance rejection performance is

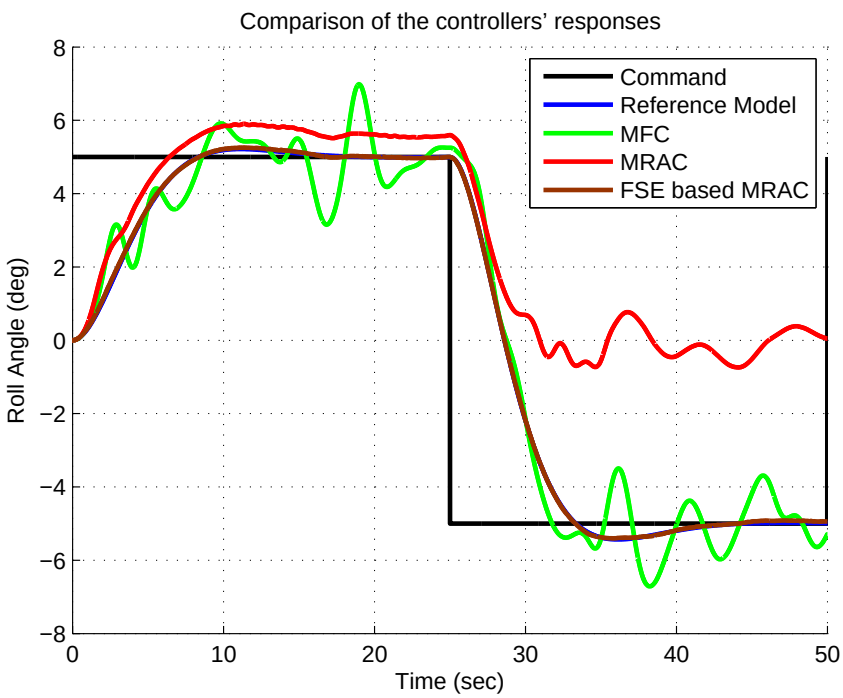

Figure 4.6: Comparison of the controllers' responses to step command.

not satisfactory.

On the other hand, the response of the Fourier series based MRAC is on the reference model roll angle. This response means that the controller acts in the desired performance level.

For the step command, the Fourier series based MRAC design is shown to be robust to the challenging disturbance case. This case is also examined using an other command set. This command set is the sine wave command as mentioned before.

The response of the Fourier series based MRAC to the sine wave roll angle command is shown in the Figure 4.7

The Figure 4.7 shows that the Fourier series based MRAC design follows the reference model roll angle. All of the effects introduced by wing rock dynamics, external disturbance and measurement noise are rejected from the response of the system. The response is clear and following the reference model.

This result shows that the proposed controller is well capable of dismissing introduced disturbances on the system.

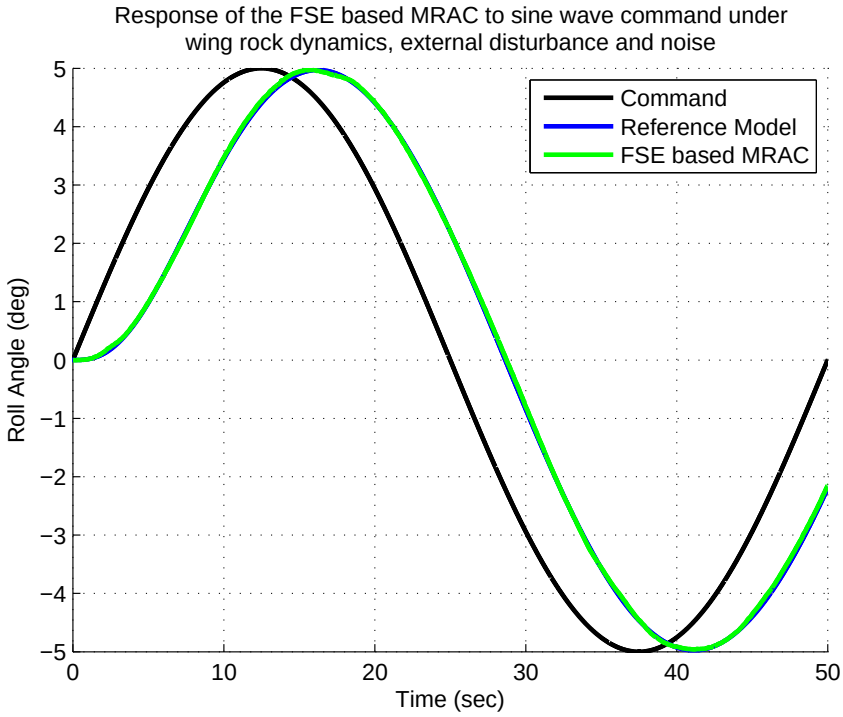

Figure 4.7: Response of the Fourier series based MRAC to sine command under the effect of wing rock dynamics, external disturbance and noise.

The simulation results for sine wave command of the MFC, the MRAC and the Fourier series based MRAC designs are compared. The comparison is shown in the Figure 4.8

In the Figure 4.8, the sine wave command is shown with the black line. The reference model roll angle is shown with the blue line. The difference between the command and reference model occurs due to the bandwidth of the reference model. The desired performance defined for the system is represented by the reference model.

The roll angle response of the MFC is shown with the green line. This response follows the reference model response with some fluctuations. These fluctuations occurs due to the effective external disturbance on the system.

The red line in the Figure 4.8 shows the response of the basic MRAC. This controllers is designed only regarding the wing rock dynamics. The MRAC design can not adapt the control input to the introduced external disturbance. Therefore, the response of it fails to follow the reference model roll angle response.

The response of the Fourier series based MRAC is shown with brown line in the

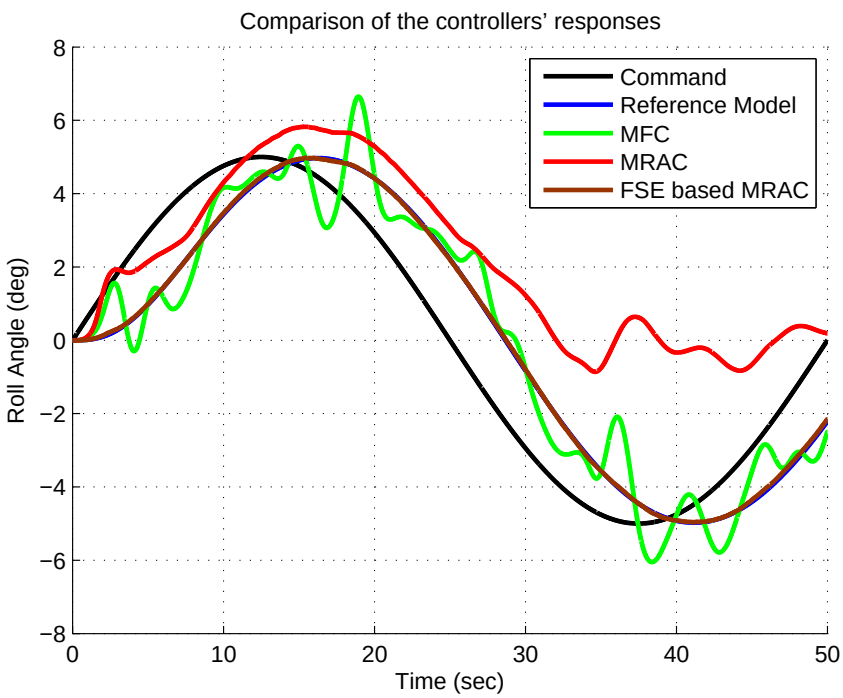

Figure 4.8: Comparison of the controllers' responses to sine command.

figure. As it can be seen from the figure, the response of the Fourier series based MRAC design follows the reference model response closely. The error done with the proposed controller is much less than the error done with the other two controllers.

4.3 Effects of Unmodeled Dynamics

In the design phase of the Fourier series based MRAC, the control actuator system dynamics are not taken into account. These dynamics are neglected. However, in applications, the dynamics regarding the control actuator system are present. Therefore, control actuation mechanism used for the controller is act as an unmodeled dynamic for the design.

The effects of the unmodeled dynamics, which is the control actuator dynamics in the present case, is examined by adding different transfer functions in the loop. The control actuator system is located between the control command and the actuated controller input.

For examination of the effect of the unmodeled dynamics on the system, four different natural frequency for the control actuator system is selected. The transfer function

regarding the control actuator system is

$$\frac{u}{u_c}(s) = \frac{\omega_c^2}{s^2 + 2\zeta_c\omega_c s + \omega_c^2}. \tag{4.45}$$

The damping ratio for the control actuator systems is kept constant. The value for the damping ratio is

$$\zeta_c = 0.7. \tag{4.46}$$

The dynamics of the control actuator system is altered by changing the natural frequency. Using higher natural frequencies result in very fast actuation so as the natural frequency increased the effect of the unmodeled dynamics is diminished. Therefore, the natural frequency selection for the unmodeled dynamics is done with in the low range of frequencies. Selected natural frequencies are

$$\omega_c = 8\ Hz \quad \omega_c = 10\ Hz \quad \omega_c = 15\ Hz \quad \omega_c = 20\ Hz. \tag{4.47}$$

The Fourier series based MRAC is examined with the control actuator systems having the selected natural frequencies. Simulations are done in order to compare the results of the each case. The response of the controller to the step command for different control actuator system natural frequencies is shown in the Figure 4.9.

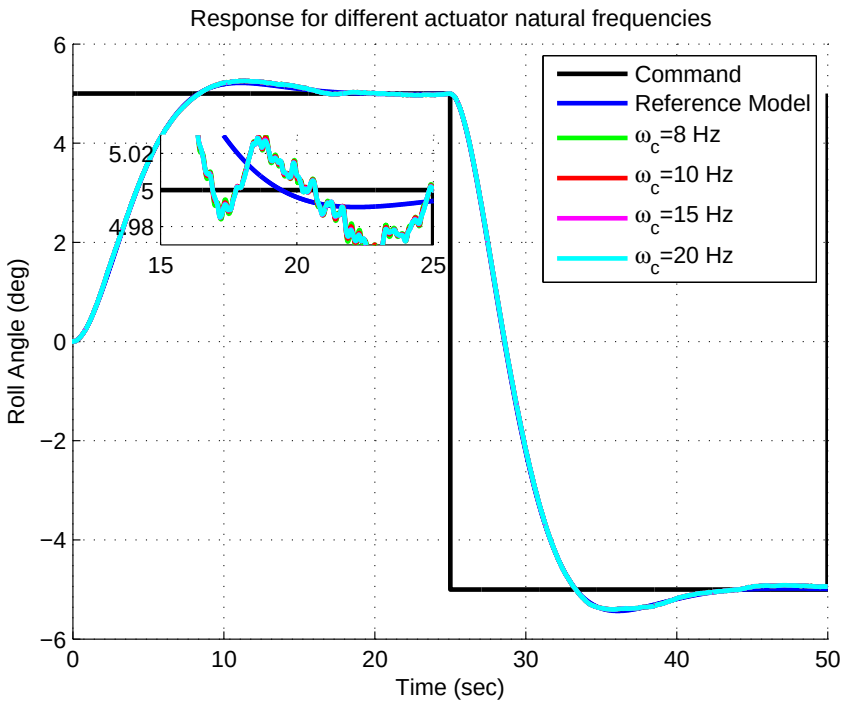

Figure 4.9: Different actuator natural frequencies.

In the Figure 4.9, the black line shows the commanded roll angle. The blue line shows response of the reference model to the commanded roll angle. The lines with the colors green, red, magenta and cyan show the response of the Fourier series based MRAC with 8 Hz, 10 Hz, 15 Hz, 20 Hz actuator system natural frequencies, respectively. The response of the controllers with different actuator natural frequencies are really close to each other.

In the figure, big scale shows the response of the controllers between 0-50 seconds of time and -6 degrees to 6 degrees roll angles. In the big scale, it is not possible to see the difference occurs due to unmodeled dynamics. In order to see the small difference between the responses, the small scale is inspected. This scale shows the time between 15 to 25 seconds and the roll angle variation between 4.98 degrees to 5.02 degrees. As can be seen from the Figure 4.9, even in the small scale, the difference between the responses of the controller for different unmodeled dynamics is really small. This plot shows that the controller is robust to unmodeled actuator dynamics.

For the actuator dynamics with higher natural frequencies, the response is almost exactly same with the responses shown in the Figure 4.9. However, for the frequencies lower than $8Hz$, the response of the controller starts to vary. After some point, the stability of the controller is lost. Therefore, this figure also shows the robustness limit of the controller for unmodeled dynamics.

4.4 Effects of Sampling Time for Fourier Series Based MRAC

The sampling time refers to the time step that the controller command is calculated as time passes. For every time step the command is calculated and actuated in order to controller the system. As the sampling time decreases, the resolution in time scale increases. Decreasing the sampling time 100 times means that the control command should be calculated 100 times more in a certain time.

The effect of the sampling time used for a controller plays an important role for real time applications. In real time applications, the processor used in the control computer need to compute all of the necessary computations for calculation of the

control command. And, all of these computations must be done in one sampling time. In case the computations can not fit in one sampling time, the control computer can not calculate the next control command and a delay due to the computation occurs. This delay is totally unwanted, therefore, proper controllers or processors for correct sampling times are selected for applications.

Controllers which can run with lower sampling times without performance or robustness loss, are stronger for real time applications. The processors that computes more operations in certain time span are more expensive. In order to have a practical controller, lower sampling times are desired.

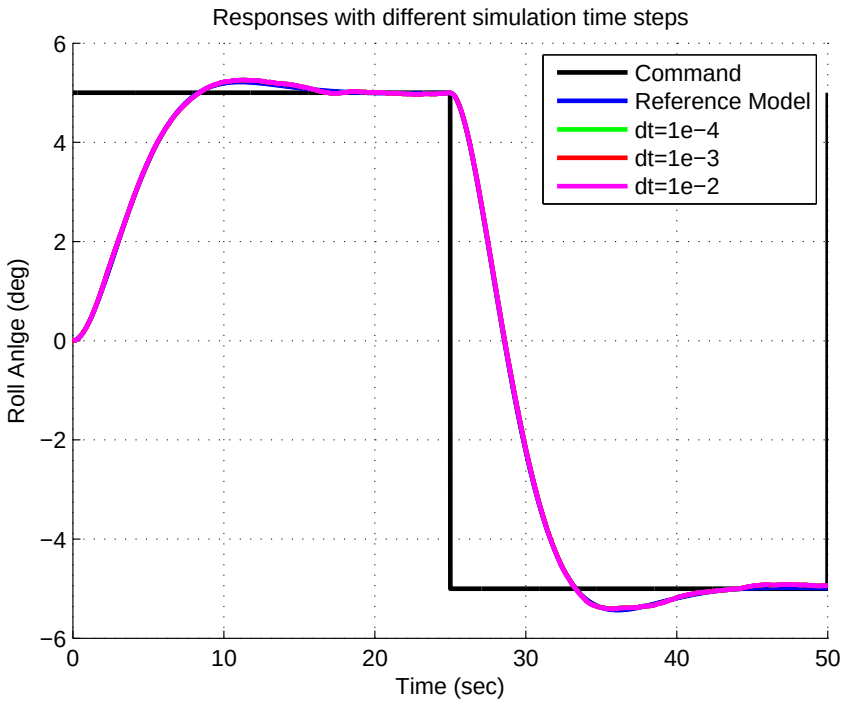

Figure 4.10: Responses with different sampling times.

The effect of the sampling time for the Fourier series based MRAC is inspected in this section. The simulation with challenging disturbance case is repeated with 3 different sampling times. These sampling times are 0.0001, 0.001 and 0.01 seconds. The response of the controller to step command is shown in the Figure 4.10.

In the Figure 4.10, the black line shows the commanded step input for the roll angle. The blue line shows the reference model response to the command. The green line shows the controller response with highest sampling time. The sampling time for this simulation is 0.1 milliseconds. The red line shows the simulation results with 1

millisecond sampling time. The magenta line has the lowest sampling time in between three simulations. The sampling time for that line is 10 milliseconds.

As it can be seen from the figure, the designed controller can perform almost exactly same with higher and lower sampling times. The response of the controller for 0.1 milliseconds sampling time and 10 milliseconds sampling time are almost on each other that it can not be selected by inspecting the Figure 4.10.

This property of the Fourier series based MRAC is very important and powerful property, since, this enables usage for practical problems. And gives possibility to use cheaper processors in applications.

4.5 Disturbance Rejection Character of Fourier Series Based MRAC

The disturbance rejection character of the model following controller is inspected in 2.3 by using analytical methods. The transfer function from disturbance input to the roll angle is calculated, and the magnitude plot of this transfer function is plotted. This magnitude plot shows how the controller acts for a certain disturbance in certain frequency. The amount of magnitude in the plot for that frequency corresponds the ratio how the controller suppress the disturbance.

This method for disturbance rejection character analysis can not be applied for the Fourier series based MRAC. The reason for that is the proposed controller contains nonlinear elements. The transfer function approach is a linear control design tool. However, a similar approach can be used to examine the disturbance rejection character of the designed controller.

The idea of inspecting the disturbance rejection character of the controller is to understand the amount of suppression done by the controller for a disturbance with certain frequency. In order to do that, periodic disturbances with different frequencies can be applied to the controller and the ratio with the output can be inspected.

There are few points need to be mentioned for this procedure. The first one is that, the controller should have no other input than the disturbance input. Therefore, commanded input, noise input or any other kind of disturbance inputs are canceled out

from the simulations. By this way, the only input into the system is set as the sinusoidal disturbance input. The next point is the amplitude of the sinusoidal disturbance on the system. In the linear controller case, the search is done only changing the frequency of the periodic disturbance. However, for the designed controller, this may result in misleading conclusions. This is because of the fact that the design Fourier series based MRAC is a nonlinear controller. In linear controller case such as MFC, the amplitude of the disturbance is not important since the response will grove linearly as the amplitude of the disturbance increases, so transfer function method can be safely used. In nonlinear controller case, the response may or may not change depending on the amplitude of the disturbance input. Therefore, the amplitude of the disturbance should also be taken into consideration.

The disturbance rejection character of the Fourier series based MRAC is inspected by using sinusoidal disturbance inputs in 20 different frequencies and 3 different amplitudes. The disturbance rejection character of the designed controller compared with the one of MFC is shown in the Figure 4.11.

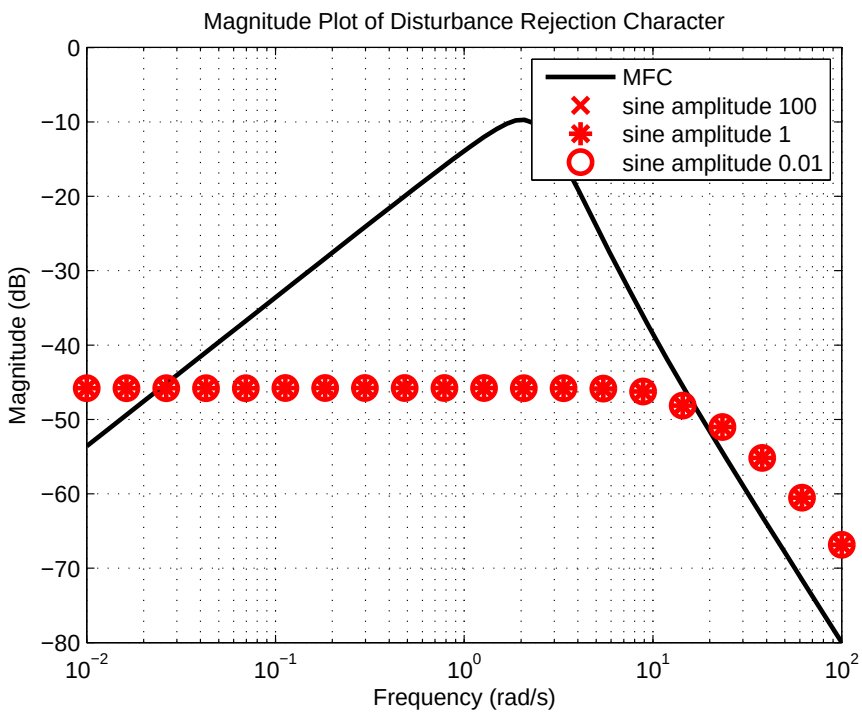

Figure 4.11: Magnitude plot of disturbance rejection character.

In the Figure 4.11, the black line shows the magnitude plot of the disturbance rejection transfer function of the controller designed using MFC method. This plot is also

shown in the Figure 2.5. The frequency range between 10^{-2} rad/s to 10^{2} rad/s is separated into 20 equally logarithmic spaced pieces. At start point of each piece the disturbance input roll angle output magnitude ratio test is applied. The results are shown with the red points for different frequency and magnitudes. The red x points shows the disturbance rejection ratio of the Fourier series based MRAC for sinusoidal input with amplitude of 100 radians for every selected frequency. The red * points represents the sinusoidal disturbance input with amplitude of 1 radians. The red o points represents the sinusoidal disturbance input with amplitude of 0.01 radians.

One result from the Figure 4.11 can be taken as the disturbance rejection character of the designed controller is linear with amplitude and frequency of the sinusoidal disturbance input within the selected range. The ratio magnitude points are turned out to be on each other for different amplitudes. This results shows the linear nature of the controller.

The other result from the magnitude plot of the disturbance rejection character of the Fourier series based MRAC is that it has a better disturbance rejection than the MFC designed for some part of the inspected frequency range. The most possible disturbance occurs in this range so it can be said that the Fourier series based MRAC is more robust to disturbances than MFC.

Before, with the simulations under challenging disturbance case, the Fourier series based MRAC is shown to be more robust to unmodeled disturbances. With the present analysis, it is also shown mathematically.

4.6 Simulations with Different Random Disturbances

The Fourier series based MRAC design is simulated under challenging disturbance case. This case includes the wing rock dynamics, the selected external disturbance and measurement noise. The performance of the controller for step command and challenging disturbance case is shown in the Figure 4.5.

The external disturbance used in challenging disturbance case is a random disturbance and shown in the Figure 2.18. The performance of the designed controllers

MFC, MRAC and Fourier series based MRAC is compared under step command and challenging disturbance case and responses are shown in the Figure 4.6.

In order to push the limits of the designed Fourier series based MRAC, the external disturbance δ_{ex} is made more challenging. Two new random disturbance are defined. These external disturbance cases are shown in the Figure 4.12.

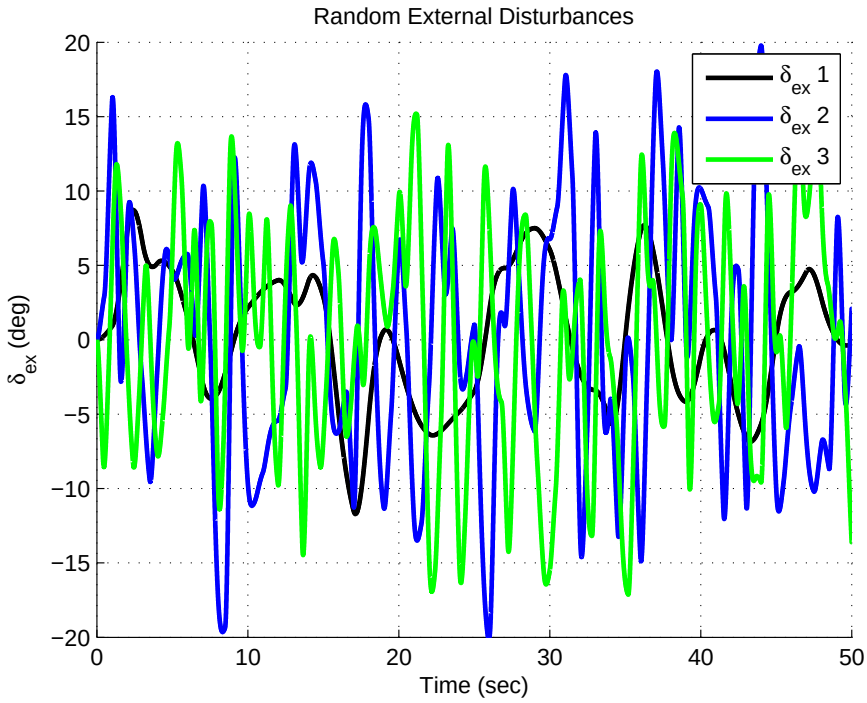

Figure 4.12: Random external disturbances.

The black line in the Figure 4.12 shows the external disturbance used in the challenging case. This disturbance is a good selection for comparison with the MFC and MRAC controllers since neither one of them becomes unstable under this disturbance. However, for the disturbance cases shown by blue and green lines in the Figure 4.12, the controller designed by using MFC and MRAC becomes unstable. As it can be seen from the Figure 4.12, the frequency content of the new defined disturbances $\delta_{ex}2$ and $\delta_{ex}3$ contains higher components.

The response of the Fourier series based MRAC under the wing rock dynamics, measurement noise and the shown external disturbances is inspected. The command to the controller is selected as the step command. The results are shown in the Figure 4.13.

In the Figure 4.13, the black line shows the commanded input, the blue line shows

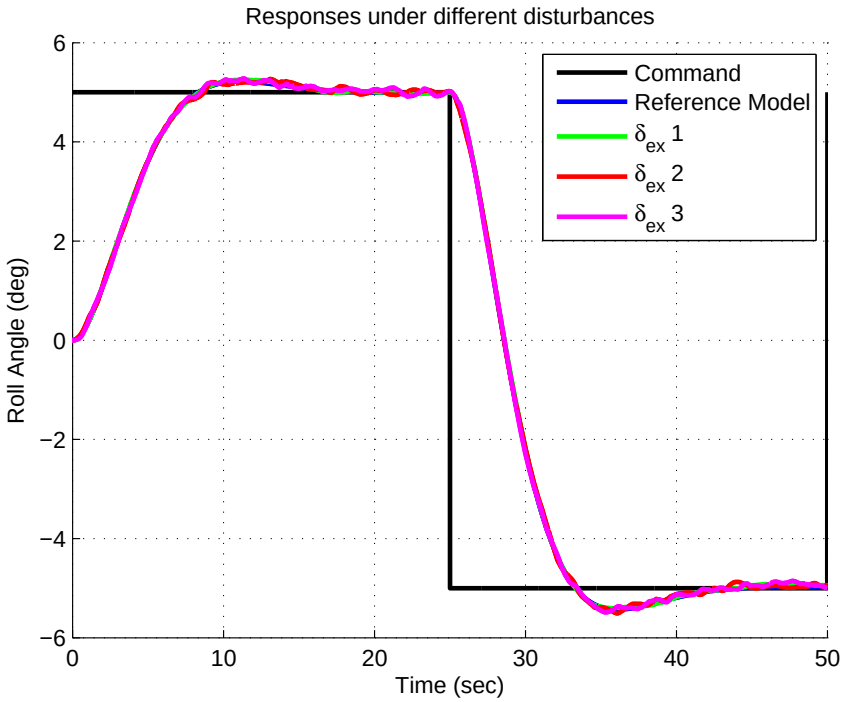

Figure 4.13: Responses under different random disturbances.

the reference model response. The green, red and magenta lines show the responses of the Fourier series MRAC under $\delta_{ex}1$, $\delta_{ex}2$ and $\delta_{ex}3$, respectively.

As it can be seen from the Figure 4.13, the design controller can diminish the effect of the challenging external disturbances and wing rock dynamics smoothly.

CHAPTER 5

CONCLUSION

In this thesis, a novel approach for adaptive control; the Fourier series based model reference adaptive control method is represented. In addition to the new approach, two controllers are designed. One of the controllers is designed using model following control, and the other one is designed using basic model reference adaptive control.

The model following controller is a method that stands in the modern control theory. A reference model is defined for the controller and states of the system are augmented with the reference model system. Finally, a full-state feedback control system is obtained. The model following controller gives ability to use well known frequency domain design tools, since itis a linear controller. These tools are Bode diagrams and magnitude plots. By using these diagrams, the bandwidth of the controller, disturbance rejection character and noise filtering property is inspected. The model following controller is designed to follow the given reference model closely in addition with having good disturbance rejection character. This controllers is used as a baseline controller for the basic model reference adaptive control and more importantly Fourier series based model reference adaptive control.

The model following controllers performance and robustness to disturbances is also examined by using simulations. For a certain case, the controller has problems with the introduced disturbance. This challenging case leads the design to adaptive control field. This case is taken as a baseline case for using to compare the other adaptive controllers.

As an adaptive controller first, the basic MRAC method is tried. The designed MRAC gives satisfactory results under certain disturbances. However, for the challenging case, the robustness of the MRAC is shown to be not fulfilling. It is inferred from the results of the challenging case simulations that the MRAC method can not deal with disturbances that are not defined in the parametrization. Therefore, an alternative for the uncertainty parametrization is needed.

The novel method of uncertainty parametrization is proposed with Fourier series based MRAC. In this method, the uncertainty parametrization is done using simple sine and cosine functions. These functions are used as universal approximators. This form of approximator is called the Fourier series expansion.

The Fourier series based MRAC is designed for the given sample system. The performance and robustness properties of the controller is examined using simulations. The challenging disturbance case which gives difficulties to the MFC and MRAC methods is tried for Fourier series based MRAC. This case is used as baseline, since the linear MFC could not succeed to overcome the introduced disturbance where the disturbance rejection character of the MFC is evaluated analytically.

The Fourier series based MRAC gives satisfactory results for the challenging case. The comparison with the MFC and the MRAC shows that the Fourier series based MRAC has better disturbance rejection character. Having better disturbance rejection character for proposed controller is a result of using Fourier series as a universal approximator for uncertainty parametrization.

Finally, it is concluded that the proposed method has promising properties for controller designs on uncertain system that are open for external disturbances.

Future studies for the proposed controller can cover sensor noise sensitivity analysis of the controller, analysis of the Fourier series parameters such as series length and period on the performance and robustness of the controller. Moreover, improvements for the controller as applying onto output feedback problems and unmatched disturbance cases are also will take place in the future works.

REFERENCES

[1] F. M. Al-Sunni and F. L. Lewis. Gain scheduling simplification by simultaneous control design. *Journal of Guidance, Control, and Dynamics*, 16:602–603, 1991.

[2] S. J. Asseo. Application of optimal control to perfect model following. *Journal of Aircraft*, 7(4):308–313, 1969.

[3] K. J. Astrom. Adaptive control around 1960. In *IEEE Conference on Decision and Control*, pages 2784–2789, 1995.

[4] K. J. Astrom and B. Wittenmark. On self tuning regulators. *Automatica*, 9(2):185 – 199, 1972.

[5] K. J. Astrom and B. Wittenmark. *Adaptive Control*. Prentice-Hall, 1994.

[6] R. Bellman. *Introduction to the Mathematical Theory of Control Processes*. Academic Press INC., 1967.

[7] R. L. Butchart and B. Shackcloth. Synthesis of model reference adaptive control systems by lyapunov's second method. In *Proceedings IFAC Symposium on Adaptive Control*, 1965.

[8] A. Calise, M. Sharma, and J. Gorban. An adaptive autopilot design for guided munitions. In *AIAA Guidance, Navigation, and Control Conference*, 1998.

[9] A. Calise, T. Yucelen, J. Muse, and B.-J. Yang. A loop recovery method for adaptive control. In *AIAA Guidance, Navigation, and Control Conference*, 2009.

[10] A. J. Calise and T. Yucelen. Adaptive loop transfer recovery. *Journal of Guidance, Control, and Dynamics*, 35:807–815, 2012.

[11] R. Chandramohan, T. Yucelen, A. Calise, G. Chowdhary, and E. Johnson. Experimental results for kalman filter modification in adaptive control. In *AIAA Infotech at Aerospace*, 2010.

[12] C.-T. Chen. *Analog and Digital Control System Design: Transfer-Function, State-Space, and Algebraic Methods*. Oxford University Press, Inc., 1995.

[13] R. Chiang, W. Breckenridge, and E. Wong. Self-tuning thruster control for cassini spacecraft. In *AIAA Guidance, Navigation, and Control Conference*, 1996.

[14] G. Chowdhary and E. N. Johnson. Adaptive neural network flight control using both current and recorded data. In *AIAA Guidance, Navigation, and Control Conference*, 2007.

[15] G. Chowdhary and E. N. Johnson. Concurrent learning for improved convergence in adaptive flight control. In *AIAA Guidance, Navigation, and Control Conference*, 2010.

[16] J. L. Crassidis and J. L. Junkins. *Optimal Estimation of Dynamic Systems*. CRC Press, 2004.

[17] I. Flgge-Lotz. Memorial to n. minorsky. *Automatic Control, IEEE Transactions on*, 16(4):289–291, 1971.

[18] R. B. Gezer and A. T. Kutay. Robust model following control design for missile roll autopilot. In *Control (CONTROL), 2014 UKACC International Conference on*, 2014.

[19] E. N. J. Girish V. Chowdhary. Theory and flight-test validation of a concurrent-learning adaptive controller. *Journal of Guidance, Control, and Dynamics*, 34:592–607, 2011.

[20] P. C. Gregory. Air research and development command plans and programs. In *Proceedings of the Self Adaptive Flight Control Symposium*, pages 8–15, 1959.

[21] R. Hess. Self-tuning generalized predictive control applied to terrain following flight. In *AIAA Guidance, Navigation, and Control Conference*, 1993.

[22] P. Ioannou and P. Kokotovic. Instability analysis and improvement of robustness of adaptive control. *Automatica*, 20(5):583 – 594, 1984.

[23] P. A. Ioannou and P. V. Kokotovic. An asymptotic error analysis of identifiers and adaptive observers in the presence of parasitics. *Automatic Control, IEEE Transactions on*, 27:921–927, 1982.

[24] P. A. Ioannou and P. V. Kokotovic. *Adaptive Systems with Reduced Models*. Springer-Verlag, 1983.

[25] P. A. Ioannou and P. V. Kokotovic. Robust redesign of adaptive control. *Automatic Control, IEEE Transactions on*, 29:202–211, 1984.

[26] R. Kalman. Design of a self-optimizing control system. *Transactions ASME*, 80:468–478, 1958.

[27] K. Kim, T. Yucelen, and A. Calise. K- modification in adaptive control. In *AIAA Infotech at Aerospace*, 2010.

[28] E. Kreindler and D. Rothschild. Model-following in linear-quadratic optimization. *AIAA Journal*, 14(7):835–842, 1976.

[29] G. Kreisselmeier and K. S. Narendra. Stable model reference adaptive control in the presence of bounded disturbances. *Automatic Control, IEEE Transactions on*, 27:1169–1175, 1982.

[30] E. Lavretsky, R. Gadient, and I. M. Gregory. Predictor-based model reference adaptive control. *Journal of Guidance, Control, and Dynamics*, 33(4):1195–1201, 2010.

[31] J. Levin, R. Gadient, and E. Lavretsky. Alternative model reference adaptive control. In *AIAA Guidance, Navigation, and Control Conference*, 2010.

[32] A. M. Lyapunov. *The general problem of the stability of motion*. PhD thesis, University of Kharkov, Kharkov Mathematical Society, Kharkov, 1892.

[33] A. M. Lyapunov. *General Problem of the Stability Of Motion*. Taylor and Francis, 1992.

[34] J. C. Maxwell. On governors. *Proceedings of the Royal Society of London*, 2:270–283, 1868.

[35] N. Minorsky. Directional stability of automatically steered bodies. *Journal of the American Society of Naval Engineers*, 34:280–309, 1922.

[36] J. F. Muller. Systematic determination of simplified gain scheduling programs. *Journal of Aircraft*, 4:529–533, 1967.

[37] K. S. Narendra and A. M. Annaswamy. A new adaptive law for robust adaptation without persistent excitation. *Automatic Control, IEEE Transactions on*, 32:134–145, 1987.

[38] N. Nguyen. Least-squares model-reference adaptive control with chebyshev orthogonal polynomial approximation. *Journal of Aerospace Information Systems*, 10(6):268–286, 2013.

[39] N. Nguyen, K. Krishnakumar, and J. Boskovic. An optimal control modification to model-reference adaptive control for fast adaptation. In *AIAA Guidance, Navigation, and Control Conference*, 2008.

[40] N. T. Nguyen. Bi-objective optimal control modification adaptive law for unmatched uncertain systems. In *AIAA Guidance, Navigation, and Control Conference*, 2013.

[41] H. Nyquist. Regeneration theory. *Bell System Technical Journal*, 11:126–147, 1932.

[42] K. Ogata. *Modern Control Engineering*. Prentice Hall, 2002.

[43] P. V. Osburn, H. P. Whitaker, and A. Kezer. New developments in the design of model reference adaptive control systems. *Institute of the Aerospace Sciences*, 1961.

[44] P. Parks. Liapunov redesign of model reference adaptive control systems. *Automatic Control, IEEE Transactions on*, 11(3):362–367, 1966.

[45] B. B. Peterson and K. S. Narendra. Bounded error adaptive control. *Automatic Control, IEEE Transactions on*, 27:1161–1168, 1982.

[46] J. B. Pomet and L. Praly. Adaptive nonlinear regulation: estimation from the lyapunov equation. *Automatic Control, IEEE Transactions on*, 37(6):729–740, 1992.

[47] L. S. Pontryagin. *The Mathematical Theory of Optimal Processes*. Gordon and Breach Science Publishers, 1962.

[48] T. Richardson, P. Davison, M. Lowenberg, and M. di Bernardo. Control of nonlinear aircraft models using dynamic state-feedback gain scheduling. In *AIAA Guidance, Navigation, and Control Conference and Exhibit*, 2003.

[49] I. M. Ross. *A Primer on Pontryagin's Principle in Optimal Control*. Collegiate Publishers, 2009.

[50] J. S. Shamma. *Analysis and Design of Gain Scheduled Control Systems*. PhD thesis, Massachusetts Institute of Technology, Cambridge, MA, 1988.

[51] L. S. Shieh, J. W. Sunkel, and X. M. Z. Z. Yuan. Self-tuning control of attitude and momentum management for the space station. *Journal of Guidance, Control, and Dynamics*, 15:17–27, 1992.

[52] L. Silverberg and M. Norris. Self-tuning algorithms for uniform damping control of spacecraft. In *Structures, Structural Dynamics and Materials Conference*, 1990.

[53] S. N. Singh, W. Yirn, and W. R. Wells. Direct adaptive and neural control of wing-rock motion of slender delta wings. *Journal of Guidance, Control, and Dynamics*, 18:25–30, 1995.

[54] G. Stein, G. L. Hartmann, and R. Hendrick. Adaptive control laws for f-8 flight test. *Automatic Control, IEEE Transactions on*, 22(5):758–767, Oct 1977.

[55] B. L. Stevens and F. L. Lewis. *Aircraft Control and Simulation*. Wiley Interscience Publication, 1992.

[56] M. Trentini and J. K. Pieper. Model-following control of a helicopter in hover. In *IEEE International Conference on Control Applications*, 1996.

[57] J. J. Tyler. The characteristics of model-following systems as synthesized by optimal control. *Automatic Control, IEEE Transactions on*, 9(4):485–498, 1964.

[58] V. Valkenburg. In memoriam: Hendrik w. bode (1905-1982). *Automatic Control, IEEE Transactions on*, 29(3):193–194, 1984.

[59] M. Verhaegen and V. Verdult. *Filtering and System Identification: A Least Squares Approach*. Cambridge University Press, 2007.

[60] H. Whitaker., J. Yamron., and A. Kezer. Design of model-reference adaptive control systems for aircraft. In *Technical Report, Instrumentation Laboratory, Massachusetts Institute of Technology*, 1958.

[61] B. T. Whitehead and S. R. Bieniawski. Model reference adaptive control of a quadrotor uav. In *AIAA Guidance, Navigation, and Control Conference*, 2010.

[62] T. Yucelen. *Advances in Adaptive Control Theory: Gradient- and Derivative-Free Approaches*. PhD thesis, Georgia Institute of Technology, Georgia, 2012.

[63] T. Yucelen and A. J. Calise. Kalman filter modification in adaptive control. *Journal of Guidance, Control, and Dynamics*, 33:426–439, 2010.

[64] T. Yucelen and A. J. Calise. Derivative-free model reference adaptive control. *Journal of Guidance, Control, and Dynamics*, 34:933–950, 2011.

[65] T. Yucelen and A. J. Calise. Robustness of a derivative-free adaptive control law. *Journal of Guidance, Control, and Dynamics*, 37:1–12, 2014.

[66] T. Yucelen and E. Johnson. Command governor-based adaptive control. In *AIAA Guidance, Navigation, and Control Conference*, 2012.

APPENDIX A

PROOF OF LYAPUNOV STABILITY OF THE WEIGHT UPDATE LAW FOR PARAMETRIC UNCERTAINTY

The Lyapunov function candidate for searching the stability bounds of the proposed controller is shown in (A.1).

$$\mathcal{V}(e(t), \tilde{W}(t)) = \frac{1}{2}e(t)^T P e(t) + \frac{1}{2}tr(\tilde{W}(t)^T \Gamma^{-1} \tilde{W}(t)) \tag{A.1}$$

The Lyapunov function $\mathcal{V}(e(t), \tilde{W}(t))$ is selected in quadratic form of its variables $e(t)$ and $\tilde{W}(t))$. The matrix $P \in \mathbb{R}^{n\times n}$ shown in (A.1) is the solution of the Lyapunov equation shown in (A.2). The matrix $\Gamma^{-1} \in \mathbb{R}^{m\times m}$ is the learning rate and design selection which is always positive definite.

$$A_m^T P + P A_m + R = 0 \tag{A.2}$$

The matrix $R \in \mathbb{R}^{n\times n}$ is a positive definite design selection which drives the Lyapunov equation.

The derivative of the Lyapunov function candidate is as follows;

$$\begin{aligned}\dot{\mathcal{V}}(e(t), \tilde{W}(t)) = \frac{1}{2}\dot{e}(t)^T P e(t) + \frac{1}{2}e(t)^T P \dot{e}(t) + \frac{1}{2}tr(\dot{\tilde{W}}(t)^T \Gamma^{-1} \tilde{W}(t)) \\ + \frac{1}{2}tr(\tilde{W}(t)^T \Gamma^{-1} \dot{\tilde{W}}(t)).\end{aligned} \tag{A.3}$$

The first two terms in (A.3) can be combined by maintaining the relation below

$$\begin{aligned}\left[\dot{e}_{(n\times1)}\right]^T P_{(n\times n)}e_{(n\times1)} &= \left[\dot{e}_{(n\times1)}\right]^T_{(1\times n)} \begin{bmatrix} P_{1(1\times n)}e_{(n\times1)} \\ \vdots \\ P_{i(1\times n)}e_{(n\times1)} \\ \vdots \\ P_{n(1\times n)}e_{(n\times1)} \end{bmatrix}_{(n\times1)} \\ &= \begin{bmatrix} P_{1(1\times n)}e_{(n\times1)} \\ \vdots \\ P_{i(1\times n)}e_{(n\times1)} \\ \vdots \\ P_{n(1\times n)}e_{(n\times1)} \end{bmatrix}^T_{(1\times n)} \qquad \dot{e}_{(n\times1)} = \left[e_{(n\times1)}\right]^T P^T_{(n\times n)}\dot{e}_{(n\times1)}.\end{aligned} \tag{A.4}$$

The relation shown in (A.4) states that if $P = P^T$ then $\dot{e}(t)^T Pe(t) = e(t)P\dot{e}(t)$. The matrix P is symmetrical since it is the solution of the Lyapunov equation shown in (A.2). The trace operator has the following property

$$tr(M) = tr(M^T) \tag{A.5}$$

So the third and fourth terms of the derivative of the Lyapunov function candidate (A.3) can be combined with the selection of the learning rate with the property; $\Gamma^{-1} = \Gamma^{-T}$. Hence, the derivative of the Lyapunov function candidate takes the following form;

$$\dot{\mathcal{V}}(e(t), \tilde{W}(t)) = e(t)^T P\dot{e}(t) + tr\left(\tilde{W}(t)^T\Gamma^{-1}\dot{\tilde{W}}(t)\right) \tag{A.6}$$

The error dynamics $\dot{e}(t)$ can be replaced with the equation shown in (4.22) implementing Assumption 4.1.2

$$\begin{aligned}\dot{\mathcal{V}}(e(t), \tilde{W}(t)) &= e(t)^T P\left(A_m e(t) - B\tilde{W}(t)^T\beta(t)\right) + tr\left(\tilde{W}(t)^T\Gamma^{-1}\dot{\tilde{W}}(t)\right) \\ &= e(t)^T PA_m e(t) - e(t)^T PB\tilde{W}(t)^T\beta(t) + tr\left(\tilde{W}(t)^T\Gamma^{-1}\dot{\tilde{W}}(t)\right).\end{aligned} \tag{A.7}$$

The first term can be expanded with the Lyapunov equation shown in (A.2) as follows;

$$\dot{\mathcal{V}}(e(t), \tilde{W}(t)) = \tfrac{1}{2}e(t)^T(A_m^T P + PA_m)e(t) - e(t)^T PB\tilde{W}(t)^T\beta(t) + tr\left(\tilde{W}(t)^T\Gamma^{-1}\dot{\tilde{W}}(t)\right). \tag{A.8}$$

And the expression $(A_m^T P + PA_m)$ can be replaced by $-R$ which gives;

$$\dot{\mathcal{V}}(e(t), \tilde{W}(t)) = -\tfrac{1}{2}e(t)^T Re(t) - e(t)^T PB\tilde{W}(t)^T\beta(t) + tr\left(\tilde{W}(t)^T\Gamma^{-1}\dot{\tilde{W}}(t)\right). \tag{A.9}$$

The matrix R is a design selection and it is always positive definite; so, the negative of it is always negative definite. The first term of (A.9) is quadratic of $e(t)$ and it is always less than zero for $e(t) \neq 0$ and zero for $e(t) = 0$. The derivative of the Lyapunov function candidate needs to be less than zero for every t to guarantee asymptotical stability. This condition dictates the remaining summation of two terms of (A.9) to be equal to zero. This relation is shown in

$$e(t)^T PB\tilde{W}(t)^T \beta(t) = tr\left(\tilde{W}(t)^T \Gamma^{-1} \dot{\tilde{W}}(t)\right). \tag{A.10}$$

The left side of the above equation can be transformed into the following form using the trace operator as follows

$$tr\left(\tilde{W}(t)^T \beta(t) e(t)^T PB\right) = tr\left(\tilde{W}(t)^T \Gamma^{-1} \dot{\tilde{W}}(t)\right). \tag{A.11}$$

The same relation holds for the inner matrices of the trace operators at both sides, so

$$\tilde{W}(t)^T \beta(t) e(t)^T PB = \tilde{W}(t)^T \Gamma^{-1} \dot{\tilde{W}}(t). \tag{A.12}$$

Simplifying $\tilde{W}(t)$ terms from both sides and keeping $\dot{\tilde{W}}(t)$ in one side gives the following equation

$$\dot{\tilde{W}}(t) = \Gamma \beta(t) e(t)^T PB. \tag{A.13}$$

The weight error is $\tilde{W}(t) = \hat{W} - W$, and the ideal weights W are constant. The derivative of the ideal weight is $\dot{W} = 0$, thus

$$\left(\dot{\hat{W}}(t) - \dot{W}(t)\right) = \dot{\hat{W}}(t) = \dot{\tilde{W}}(t) = \Gamma \beta(t) e(t)^T PB. \tag{A.14}$$

From the above equation, the final form of the weight update law is

$$\dot{\hat{W}}(t) = \Gamma \beta(t) e(t)^T PB \tag{A.15}$$

with the Lyapunov function properties

$$\mathcal{V}(e(t), W(t)) \geq 0 \quad and \quad \dot{\mathcal{V}}(e(t), W(t)) \leq 0. \tag{A.16}$$

So the controller

$$u = u_n - u_{ad} = -K_1 x(t) + K_2 r(t) - \hat{W}^T \beta(t) \tag{A.17}$$

is stable with the weight update law shown in (A.15) and under the Assumption 4.1.2 $(\varepsilon = 0)$.

APPENDIX B

PROOF OF LYAPUNOV STABILITY OF THE WEIGHT UPDATE LAW FOR NON-PARAMETRIC UNCERTAINTY

For stability proof, the same Lyapunov function candidate shown in (A.1) is used. The derivative of the Lyapunov function candidate is the same with (A.6). Placing the error dynamics shown in (4.22), and the weigth update law shown in (4.29) into (A.6) gives the following equation

$$\begin{aligned}\dot{\mathcal{V}}(e(t),\tilde{W}(t)) = e(t)^T P\left(A_m e(t) - B\tilde{W}(t)^T\beta(t) + B\varepsilon(t)\right)\\ + tr\left(\tilde{W}(t)^T\Gamma^{-1}\Gamma\left(\beta(t)e(t)^T PB - \sigma\hat{W}(t)\right)\right).\end{aligned} \tag{B.1}$$

This equation simplifies to

$$\begin{aligned}\dot{\mathcal{V}}(e(t),\tilde{W}(t)) = \left(e(t)^T PA_m e(t) - e(t)^T PB\tilde{W}(t)^T\beta(t) + e(t)^T PB\varepsilon(t)\right)\\ + tr\left(\tilde{W}(t)^T\beta(t)e(t)^T PB - \tilde{W}(t)^T\sigma\hat{W}(t)\right).\end{aligned} \tag{B.2}$$

The term $e(t)^T PB\tilde{W}(t)^T\beta(t)$ is equal to the term $tr\left(\tilde{W}(t)^T\beta(t)e(t)^T PB\right)$ so the equation is

$$\dot{\mathcal{V}}(e(t),\tilde{W}(t)) = e(t)^T PA_m e(t) + e(t)^T PB\varepsilon(t) - tr\left(\tilde{W}(t)^T\sigma\hat{W}(t)\right). \tag{B.3}$$

By using the Lyapunov equation shown in (A.2),the term $e(t)^T PA_m e(t)$ can be replaced with $-\frac{1}{2}e(t)^T Re(t)$ and the equation takes the form

$$\dot{\mathcal{V}}(e(t),\tilde{W}(t)) = -\frac{1}{2}e(t)^T Re(t) + e(t)^T PB\varepsilon(t) - \sigma tr\left(\tilde{W}(t)^T\hat{W}(t)\right). \tag{B.4}$$

The estimated weight $\hat{W}(t)$ in (B.4) can be replaced with the summation of weight error and perfect weight $\tilde{W}(t) + W$.

$$\dot{\mathcal{V}}(e(t),\tilde{W}(t)) = -\frac{1}{2}e(t)^T Re(t) + e(t)^T PB\varepsilon(t) - \sigma tr\left(\tilde{W}(t)^T(\tilde{W}(t) + W)\right). \tag{B.5}$$

The above equation can be reorganized as follows

$$\dot{\mathcal{V}}(e(t),\tilde{W}(t)) = -\tfrac{1}{2}e(t)^T Re(t) - \sigma tr\left(\tilde{W}(t)^T\tilde{W}(t)\right) + e(t)^T PB\varepsilon(t) + tr\left(\tilde{W}(t)^T W\right). \quad \text{(B.6)}$$

In order to prove the stability of the proposed modification, the bounds for derivative of the Lyapunov function candidate is less than zero should be found. For this purpose, each term of (B.6) is examined. The first term in (B.6) has the following relation

$$-\frac{1}{2}e(t)^T Re(t) \leq -\frac{1}{2}\lambda_{min}(R)e(t)^T e(t) = -\frac{1}{2}\lambda_{min}(R)\|e(t)\|_2^2. \quad \text{(B.7)}$$

where $\|.\|_2$ stands for the Euclidian norm of a vector, and λ_{min} is the minimum eigenvalue of the matrix R. The Frobenius norm $\|.\|_F$ of a matrix is equal to the square root of the trace of the multiplication of its transpose and itself. So by using the definition of the Frobenius norm the second term in (B.6) can be rewritten as

$$-\sigma tr\left(\tilde{W}(t)^T\tilde{W}(t)\right) = -\sigma\|\tilde{W}(t)\|_F^2. \quad \text{(B.8)}$$

By assigning an upper bound ε^* for error of the representation of the uncertainty by the Fourier series expansion, and using the Euclidian and Frobenius norms the third term in (B.6) can be bounded with the following inequality

$$e(t)^T PB\varepsilon(t) \leq \varepsilon^*\|PB\|_F\|e(t)\|_2. \quad \text{(B.9)}$$

Finally, the fourth term in (B.6) has the following relation

$$\sigma tr\left(\tilde{W}(t)^T W\right) \leq \sigma\|W\|_F\|\tilde{W}(t)\|_F \quad \text{(B.10)}$$

Combining the relations (B.7), (B.8), (B.9) and (B.10) gives

$$\begin{aligned}\dot{\mathcal{V}}(e(t),\tilde{W}(t)) \leq &-\frac{1}{2}\lambda_{min}(R)\|e(t)\|_2^2 - \sigma\|\tilde{W}(t)\|_F^2 + \varepsilon^*\|PB\|_F\|e(t)\|_2 \\ &+ \sigma\|W\|_F\|\tilde{W}(t)\|_F.\end{aligned} \quad \text{(B.11)}$$

The right side of the inequality contains two second order polynomials of the variables $\|e(t)\|_2$ and $\|\tilde{W}(t)\|_F$. These polynomials can be transformed to square of differences.

$$\begin{aligned}\dot{\mathcal{V}}(e(t),\tilde{W}(t)) \leq &-\left(\left(\sqrt{\frac{1}{2}\lambda_{min}(R)}\|e(t)\|_2\right)^2 - \varepsilon^*\|PB\|_F\|e(t)\|_2 + \left(\frac{\varepsilon^*\|PB\|_F}{2\sqrt{\frac{1}{2}\lambda_{min}(R)}}\right)^2\right) \\ &-\left(\left(\sqrt{\sigma}\|\tilde{W}(t)\|_F\right)^2 - \sigma\|W\|_F\|\tilde{W}(t)\|_F + \left(\frac{\sigma\|W\|_F}{2\sqrt{\sigma}}\right)^2\right) \\ &+\left(\frac{\varepsilon^*\|PB\|_F}{2\sqrt{\frac{1}{2}\lambda_{min}(R)}}\right)^2 + \left(\frac{\sigma\|W\|_F}{2\sqrt{\sigma}}\right)^2\end{aligned} \quad \text{(B.12)}$$

So that is

$$\dot{\mathcal{V}}(e(t),\tilde{W}(t)) \leq -\left(\sqrt{\frac{1}{2}\lambda_{min}(R)}\|e(t)\|_2 - \frac{\varepsilon^*\|PB\|_F}{2\sqrt{\frac{1}{2}\lambda_{min}(R)}}\right)^2 - \left(\sqrt{\sigma}\|\tilde{W}(t)\|_F - \frac{\sigma\|W\|_F}{2\sqrt{\sigma}}\right)^2 + \left(\frac{\varepsilon^*\|PB\|_F}{2\sqrt{\frac{1}{2}\lambda_{min}(R)}}\right)^2 + \left(\frac{\sigma\|W\|_F}{2\sqrt{\sigma}}\right)^2 \tag{B.13}$$

The terms $-\left(\sqrt{\frac{1}{2}\lambda_{min}(R)}\|e(t)\|_2 - \frac{\varepsilon^*\|PB\|_F}{2\sqrt{\frac{1}{2}\lambda_{min}(R)}}\right)^2$ and $-\left(\sqrt{\sigma}\|\tilde{W}(t)\|_F - \frac{\sigma\|W\|_F}{2\sqrt{\sigma}}\right)^2$ are always negative or zero so this relation gives two bounds. One bound is for the value of the variable $e(t)$ and the other bound is for $\tilde{W}(t)$. For $e(t)$ if

$$\|e(t)\|_2 \geq \sqrt{\left(\frac{\varepsilon^*\|PB\|_F}{\lambda_{min}(R)}\right)^2 + \frac{\left(\frac{\sigma\|W\|_F}{2\sqrt{\sigma}}\right)^2}{\frac{1}{2}\lambda_{min}(R)}} + \frac{\varepsilon^*\|PB\|_F}{\lambda_{min}(R)} \tag{B.14}$$

then for any value of $\|\tilde{W}(t)\|_F$ the derivative of the Lyapunov function candidate has the relation $\dot{\mathcal{V}}(e(t),\tilde{W}(t)) \leq 0$. Similarly for $\tilde{W}(t)$ if

$$\|\tilde{W}(t)\|_F \geq \sqrt{\frac{\left(\frac{\varepsilon^*\|PB\|_F}{2\sqrt{\frac{1}{2}\lambda_{min}(R)}}\right)^2}{\sigma} + \left(\frac{\|W\|_F}{2}\right)^2} + \frac{\|W\|_F}{2} \tag{B.15}$$

then for any value of $e(t)$ the derivative of the Lyapunov function candidate has the relation $\dot{\mathcal{V}}(e(t),\tilde{W}(t)) \leq 0$. So if the relations (B.14) or (B.15) hold then then the Lyapunov function candidate with the modified weight update law satisfies the necessary relations for bounded stability which are

$$\mathcal{V}(e(t),W(t)) \geq 0 \quad and \quad \dot{\mathcal{V}}(e(t),W(t)) \leq 0. \tag{B.16}$$

The statement in (B.16) concludes the stability proof of the Fourier series expansion based model reference adaptive control method.